NASA
TP
2096
c.1

NASA Technical Paper 2096

March 1983

Studies of Sidewall Boundary Layer in the Langley 0.3-Meter Transonic Cryogenic Tunnel With and Without Suction

A. V. Murthy,
Charles B. Johnson,
Edward J. Ray,
Pierce L. Lawing,
and Jerry J. Thibodeaux

NASA

**NASA
Technical
Paper
2096**

1983

Studies of Sidewall Boundary Layer in the Langley 0.3-Meter Transonic Cryogenic Tunnel With and Without Suction

A. V. Murthy,
Charles B. Johnson,
Edward J. Ray,
Pierce L. Lawing,
and Jerry J. Thibodeaux
Langley Research Center
Hampton, Virginia

SUMMARY

An experimental and theoretical study has been made of the sidewall boundary layer with and without suction in the Langley 0.3-Meter Transonic Cryogenic Tunnel 0.3-m TCT). Without suction, the boundary-layer displacement thickness at a location ahead of the model location varied from about 1.6 to 1.3 mm over a Reynolds number range from 20 to 200 × 10^6 per meter at Mach numbers from 0.30 to 0.76. Measured velocity profiles were correlated by using the defect law of Hama, which was modified in terms of displacement thickness. The boundary-layer displacement thickness decreased when suction was applied; however, after suction of about 2 percent of the test-section mass flow, the change in thickness was small. A comparison of the measured suction effectiveness with finite-difference and integral methods of boundary-layer calculation showed that both methods predicted the right trend over the range of ratios of average suction velocity to free-stream velocity v_w/u_e up to -0.02, with the finite-difference calculation giving better agreement with the experimental data.

INTRODUCTION

Currently, an extensive, advanced-technology, airfoil testing program is in progress in the Langley 0.3-Meter Transonic Cryogenic Tunnel (0.3-m TCT) to generate high Reynolds number wind-tunnel data on two-dimensional airfoils. (See ref. 1.) The use of cryogenic nitrogen as the test gas in the 0.3-m TCT has made possible the testing of airfoils at high Reynolds numbers of practical interest. However, to gain full advantage of the high Reynolds number capability of the 0.3-m TCT, it is necessary that the interference effects caused by the finite test-section boundaries be kept to an acceptably low value or be suitably accounted for.

The interference effects of the top and bottom walls in two-dimensional testing are primarily inviscid in nature and can be corrected theoretically; when not correctable, they can be minimized by using self-streamlining wall shapes. (See ref. 2.) The intersection of the airfoil with the tunnel sidewalls gives rise to a local three-dimensional flow field because of the interaction of the approaching sidewall boundary layer with the airfoil pressure field which can seriously affect the two-dimensionality of the flow over the model. In addition, the change in the sidewall boundary-layer thickness above and below the airfoil along the chord leads to variations in the width of the flow passage and results in different effective flow Mach numbers. Recently, methods to account for this channeling effect have been proposed for the case when the sidewall boundary layer remains attached. (See refs. 3 and 4.) However, when the sidewall boundary layer is thick, it can separate even when the airfoil boundary layer is attached as in the case of low incidences at transonic speeds. The tendency for the sidewall boundary layer to separate can be minimized, and the boundary layer can be made to remain attached over a wider range of test conditions by reducing its thickness through suction or by using other types of boundary-layer-control techniques.

Recently, a sidewall boundary-layer control (BLC) system which employs suction through perforated plates was installed in the 0.3-m TCT to reduce the thickness of the sidewall boundary layer upstream of the airfoil. To evaluate the effectiveness

of the BLC system, an investigation was conducted over a wide range of operating conditions with no model present in the test section. The purpose of this paper is to describe the suction method that was employed and the results of the boundary-layer measurements used to assess the effectiveness of suction, in addition to presenting correlations of the data and comparisons with theoretical predictions. The tests covered a Mach number range from 0.30 to 0.76 and a Reynolds number range from 20 to 200 × 10^6 per meter. In contrast to the customary practice of using sintered woven screen materials for the porous media, the present method used relatively thin perforated plates with closely spaced holes. Reference 5 questioned the applicability of the standard boundary-layer prediction methods with mass transfer to calculate the growth over a closely spaced discrete-suction configuration rather than having continuous suction. This issue was examined by comparing the data presented herein with standard boundary-layer prediction methods using the assumption of continuous suction.

SYMBOLS

A	area
A^+	damping constant in equation (3)
a,b	constant in equation (4)
C_f	skin-friction coefficient, $2\tau_w/\rho_e u_e^2$
$C_{f,0}$	skin-friction coefficient without suction in equation (19)
c_p	specific heat at constant pressure
H	shape parameter, $\delta*/\theta$
$\bar{H}$	shape parameter in transformed coordinates (see eq. (8))
K	constant in skin-friction relation (see eq. (19))
k	coefficient of thermal conductivity
L	length of perforated plate in direction of flow, mm
ℓ_m	mixing length (see eq. (2))
M	Mach number
ΔM	change in Mach number across perforated plate, $M_2 - M_1$
$\dot{m}$	mass-flow rate
N_{Pr}	Prandtl number, $\mu_e c_p/k$
p	pressure, atm (1 atm = 101.3 kPa)
R	unit Reynolds number
$\bar{R}$	open-area ratio of perforated plate

R_x	Reynolds number based on x
R_θ	Reynolds number based on θ
r	recovery factor
T	temperature, K
$\bar{T}$	reference temperature (see eq. (11))
u,v	velocities parallel and normal to wall, respectively
u_τ	wall friction velocity, $\sqrt{\tau_w/\rho}$
x,y	Cartesian coordinates along and normal to wall, respectively
y^+	transformed coordinate normal to wall, $u_\tau y/\nu$
y_R	height of boundary-layer rake, 15 mm
z	$= \ln R_\theta$
α	viscosity-temperature exponent, $\mu \propto T^\alpha$
γ	ratio of specific heats
δ	boundary-layer thickness
δ^*	boundary-layer displacement thickness, $\int_0^\delta \left(1 - \dfrac{\rho u}{\rho_e u_e}\right) dy$
$\Delta\delta^*$	increase in displacement thickness across perforated plate, $\delta_2^* - \delta_1^*$
θ	boundary-layer momentum thickness, $\int_0^\delta \dfrac{\rho u}{\rho_e u_e}\left(1 - \dfrac{u}{u_e}\right) dy$
$\bar{\theta}$	boundary-layer momentum thickness in transformed plane (see eq. (7))
$\Delta\theta$	change in momentum thickness across perforated plate, $\theta_2 - \theta_1$
μ	viscosity
ν	kinematic viscosity
ρ	density
τ	shear stress

Subscripts:

aw	adiabatic wall
bl	boundary-layer bleed (i.e., removal)
e	local external conditions
i	incompressible
p	perforated plate
t	total values
ts	test section
w	wall conditions
0	free-stream stagnation conditions
1	upstream of perforated plate
2	downstream of perforated plate

Abbreviations:

BL	boundary layer
BLC	boundary-layer control
SW1,SW2	tunnel right-hand and left-hand sidewalls, respectively

EXPERIMENTAL APPARATUS

The Langley 0.3-m TCT is a closed-circuit, fan-driven tunnel using cryogenic nitrogen as a test gas. (See fig. 1.) The tunnel circuit is constructed of aluminum alloy and is thermally insulated. Under steady operating conditions of a given temperature and pressure, the heat of compression imparted to the test gas by the fan is removed by the injection of liquid nitrogen (LN_2) into the tunnel circuit and the stagnation pressure is maintained by controlling the gaseous nitrogen exhaust from the tunnel circuit.

The two-dimensional insert (ref. 6) of the 0.3-m TCT has a test-section size of 20 cm by 60 cm and has provision for removable model-mounting modules. For the sidewall BLC tests, perforated plates were fitted upstream of the model location on both sidewalls. (See fig. 2.) The quantity of boundary-layer mass flow removed from either of the sidewalls can be controlled independently by digital valves. (See refs. 7, 8, and 9.) A schematic drawing of the sidewall BLC system is shown in figure 3. The digital valve essentially consists of a number of calibrated binary-weighted sonic nozzles operating in a bistable mode either open or closed. These sonic nozzles are used in appropriate combinations to give the required flow area. The 11-bit digital valve incorporated in the present system was microprocessor controlled and had a resolution of 1 in 2048. Presently, the BLC system is operative in the passive mode and discharges bleed flow to the atmosphere. Thus, the bleed

operation is effective only for conditions for which the test-section static pressure is higher than the ambient value. Also, the maximum boundary-layer mass-removal rates will be limited to the quantity of liquid nitrogen injected in order to maintain steady operating conditions. At higher Mach numbers, the heat of compression is large; therefore, the liquid nitrogen injection rate will be higher and correspondingly higher bleed rates can be obtained. At the highest Mach number tested (M_{ts} = 0.76), up to 2.4 percent of the test-section mass flow was removed, thus giving ratios of average suction velocity to free-stream velocity v_w/u_e up to −0.02 on the perforated suction panel.

The 0.75-mm-thick aluminum-alloy perforated plates used as suction media had a nominal porosity of 20 percent and had holes of 0.25-mm diameter and 0.5-mm spacing. (See fig. 4.) This configuration of the hole geometry was based on the analysis of Streett (ref. 5), which accounts for the inviscid-sink effect due to holes by the potential-flow method. The holes were drilled by using an electron-beam technique and were given a slight divergence in the suction direction to improve pressure recovery. After drilling the holes, the plate surface was etched to obtain a smooth finish devoid of local burrs. The perforated plates were developed after considerable effort to obtain a uniform suction distribution with minimum pressure loss. A good surface finish was achieved to avoid adverse boundary-layer growth due to surface roughness when no suction is employed. The plates were mounted on a reinforced honeycomb base by using an adhesive bond to provide adequate strength to withstand operating loads.

The boundary-layer measurements were made on both sidewalls at two locations, one ahead of the perforated plate and the other behind. The measurements were made with a fixed rake having 15 total-pressure tubes equally spaced 1.0 mm apart. The first tube of the rake was at a distance of approximately 0.05δ from the wall. The configuration of the rake probes was adequate to get reliable estimates of the displacement and momentum thicknesses. The probe tips were made of stainless-steel tubing with a 0.5-mm probe outside diameter and 0.125-mm wall thickness. The location of the rakes with respect to the perforated plates on the sidewalls is shown in figure 5. The static-pressure distribution measured along the sidewall provided information on the mild adverse pressure gradient established across the suction region because of mass removal.

THEORETICAL PROCEDURES

The growth of a turbulent boundary layer over a perforated plate with discrete suction is more complicated than that over a uniformly porous wall. Particularly, the increase in boundary-layer thickness in the absence of suction can be more than that over a solid wall because of open-area effects when the hole size is large. Even when care is taken to obtain a smooth surface finish on the flow side, the free-jet-type mixing along perforations leads to a rapid growth of the boundary layer. In addition, because of the development of thin elementary boundary layers at each hole, the resistance over the solid portions of the wall will be much higher.

In the design of transonic wind tunnels with perforated walls (ref. 10), the adverse boundary-layer growth is minimized by applying suction. The suction required to keep the static pressure in the perforated-wall test section constant can be reasonably estimated, based on the shear layer growth on the walls and on tunnel mass-flow continuity considerations. (See ref. 10.) This simple approach was found to give good agreement both with preliminary measurements made earlier on a perforated wall in the 0.3-m TCT over a limited range of boundary-layer mass-flow removal

5

and with the predictions of Streett's method (ref. 5) which accounts for the inviscid-sink effects in conjunction with a boundary-layer integral method.

It is argued in reference 5 that the standard boundary-layer methods inclusive of the finite-difference methods are inadequate to predict the boundary-layer growth over perforated plates with closely spaced holes because of rapidly fluctuating velocity components produced by the discrete-suction points. However, as long as the hole diameter and the spacing are small compared to the local boundary-layer thickness, the perforated plate can be idealized by a continuous-suction surface to a first approximation. The influence of discontinuous suction on potential flow due to discrete-suction points results in the introduction of a periodic pressure field, and this effect has been studied in detail by Wuest (ref. 11) for slots and periodic perforations on a flat plate. Wuest points out that the effect of discontinuous suction decays rapidly in a distance of about half the minimum hole spacing which is 0.25 mm for the perforated plate used in the present tests. This spacing corresponds to about 2 percent of the approaching boundary-layer thickness. Furthermore, in the region close to the wall it is likely that the viscous effects may further tend to reduce the nonuniformities due to discontinuous suction. It is assumed that the outer region of the boundary layer is not significantly influenced by the individual holes and can be treated as a flow over a fictitious wall with average shear force determined by the average suction velocity over the perforated plate. The average suction velocity v_w is given by

$$\frac{\rho_w v_w}{\rho_e u_e} = - \frac{\dot{m}_{bl}}{\dot{m}_{ts}} \frac{A_{ts}}{2A_p} \tag{1}$$

In the following sections, two analytical boundary-layer prediction methods will be examined and compared with the measurements.

Finite-Difference Method

The program of Bushnell, Beckwith, and Hixon (refs. 12 and 13) was chosen from several computer codes that use grid methods for boundary-layer analysis. The measured boundary-layer profiles ahead of the suction region were used as a starting point for the calculation. The program uses an implicit finite-difference procedure to solve the mean compressible boundary-layer equations for the case of an ideal gas with constant specific heat. Deviations of boundary-layer parameters for cryogenic nitrogen gas at adiabatic conditions from the ideal-gas calculations are shown to be within about ±1 percent (ref. 14) and, hence, the present calculations have been performed with the ideal-gas assumption. The method treats the flow by considering an eddy-viscosity model based upon a mixing-length formulation. The mixing length ℓ_m is exponentially damped near the wall as

$$\ell_m = \left[1 - \exp\left(y^+/A^+\right)\right] f\left(x, \frac{y}{\delta}\right) \tag{2}$$

where $f\left(x, \frac{y}{\delta}\right)$ is the mixing-length function defined in reference 13. The value of A^+, the damping constant, is 26 for no suction. For the blowing or suction case,

6

A^+ has been correlated with experimental values of $2\rho_w v_w / \rho_e u_e C_f$ by Bushnell and Beckwith. (See ref. 13.) Analytical expressions for A^+ which include effects of both pressure gradient and mass transfer have been given by Cebeci. (See ref. 15.) For a flat-plate flow with mass transfer, A^+ is given by

$$A^+ = 26 \exp(-5.9 v_w / u_\tau) \tag{3}$$

Either equation (3) or the faired curve suggested by Bushnell and Beckwith (ref. 13) can be used. The final integral parameters calculated were about the same for either value of A^+ used. The calculated velocity profiles from the pitot-tube measurements were used as starting-input data. In the inner region near the wall, where there were no measurements, a suitable analytical profile was used. The program requires at least four steps in the linear portion of the profile. The input data in the linear region were obtained by first estimating the local skin friction and then calculating the corresponding friction velocity u_τ. The height of the linear portion of the sublayer was taken to be approximately $y^+ = 5$. For the inner region, a faired curve based on the law of the wall was employed. The local skin friction was calculated by using the incompressible expression of Thompson (ref. 16)

$$C_f = \exp(aH + b) \tag{4}$$

where

$$a = 0.019521 - z[0.386768 - z(0.028345 - 0.0007017z)]$$

$$b = 0.191511 - z[0.834891 - z(0.062588 - 0.001953z)]$$

$$z = \ln R_\theta$$

The compressibility correction for C_f for the range of test-section Mach numbers was quite small, and the simple correction (ref. 17)

$$\frac{C_f}{C_{f,i}} = \left(1 + r \frac{\gamma - 1}{4} M_e^2\right)^{-1+(1+\alpha)n} \tag{5}$$

was used, where α is the viscosity-temperature exponent, r is the recovery factor, and n is the exponent in the incompressible skin-friction law

$$C_f = (\text{Constant}) R_x^{-n} \tag{6}$$

Integral Method

Integral methods offer great simplicity in the solution of boundary-layer problems. For the case of suction with mild adverse pressure gradient, the accuracy of

prediction of the boundary-layer growth with suction depends on the type of skin-friction law used. Towne (ref. 18) has examined the application of different skin-friction laws for the different cases and has found the skin-friction law of Thompson (ref. 16), based on a three-parameter family of velocity profiles, to give good results for small suction rates. Because of the space limitation (i.e., small surface area of porous plates), much higher bleed rates existed for the tests in the 0.3-m TCT, and these results provided a means to check the validity of the skin-friction law of reference 16 for higher bleed rates. The integral equations used in the present report are the transformed momentum and moment-of-momentum expressions developed by Sasman and Cresci (ref. 19), which were modified by Towne (ref. 18) to include effects of mass transfer at the wall. These equations are, for two-dimensional flow,

$$\frac{d\bar{\theta}}{dx} = -\frac{\bar{\theta}}{M_e}\frac{dM_e}{dx}\left(2 + \frac{T_w}{T_0}\bar{H}\right) + \frac{p_e}{p_0}\frac{T_0}{T_w}\left(\frac{T_e}{T_0}\right)^{1/2}\frac{v_w}{u_e} + \left(\frac{T_e}{T_0}\right)^{\frac{\gamma+1}{2(\gamma-1)}}\frac{c_f}{2} \tag{7}$$

$$\frac{d\bar{H}}{dx} = -\frac{1}{2M_e}\frac{dM_e}{dx}\left[\bar{H}(\bar{H}+1)^2(\bar{H}-1)\right]\left[1 + \left(\frac{T_w}{T_0} - 1\right)\frac{\bar{H}^2 + 4\bar{H} - 1}{(\bar{H}+1)(\bar{H}+3)}\right]$$

$$- \frac{0.011}{\bar{\theta}}(\bar{H}+1)\left(\bar{H}^2 - 1\right)\left(\frac{\bar{H}-1}{\bar{H}}\right)^2\frac{T_0}{T_w}\left(\frac{T_e}{T_0}\right)^{\frac{\gamma+1}{2(\gamma-1)}}$$

$$+ \frac{(\bar{H}^2 - 1)\bar{H}}{\bar{\theta}}\left(\frac{T_e}{T_0}\right)^{\frac{\gamma+1}{2(\gamma-1)}}\frac{c_f}{2} + \frac{\bar{H}^2 - 1}{\bar{\theta}}\frac{p_e}{p_0}\frac{T_0}{T_w}\left(\frac{T_e}{T_0}\right)^{1/2}\frac{v_w}{u_e} \tag{8}$$

In equations (7) and (8), $\bar{\theta}$ and $\bar{H}$ refer to the values of the momentum thickness and the shape parameter, respectively, in the transformed coordinates and are given by

$$\bar{\theta} = \theta\left(\frac{T_e}{T_0}\right)^{\frac{\gamma+1}{2(\gamma-1)}} \tag{9}$$

$$H = \frac{T_w}{T_0}\bar{H}\left(1 + \frac{\gamma-1}{2}M_e^2\right) + \frac{\gamma-1}{2}M_e^2 \tag{10}$$

Also, $\bar{T}$ is the reference temperature calculated by using

$$\frac{\bar{T}}{T_0} = 0.5 \frac{T_w}{T_0} + 0.22 N_{Pr}^{1/3} + \left(0.5 - 0.22 N_{Pr}^{1/3}\right) \frac{T_e}{T_0} \qquad (11)$$

The first term on the right-hand side of equation (7) represents the pressure-gradient effects in the x-direction. The second and third terms account for the suction effects and growth due to skin friction, respectively. To integrate equations (7) and (8), the skin-friction law of reference 16 was used. The relevant expressions are

$$C_f = \exp(aH + b) \qquad (12)$$

For $\dfrac{v_w}{u_e} = -0.005$,

$$a = 1.07085 - z[0.831747 - z(0.106843 - 0.004428z)]$$

$$b = -2.338049 + z[0.015834 - z(0.047968 - 0.003308z)]$$

and for $\dfrac{v_w}{u_e} = -0.01$,

$$a = -1.00747 - \exp(10.97531 - 8.1080555 \ln z)$$

$$b = 110.92 \exp(-1.06z) - 2.94$$

$$z = \ln R_\theta$$

For intermediate values of v_w/u_e, linear interpolation was used. For higher bleed rates, the skin friction increased linearly (ref. 16) and, hence, C_f values were obtained by extrapolation. By using the initial values of momentum thickness and the shape factor from measurements, equations (7) and (8) were integrated by employing a fourth-order, variable-interval Runge-Kutta method.

Reduction of Experimental Data

The total pressures measured by the boundary-layer rake were first converted to local Mach numbers by using the one-dimensional relation

$$M^2 = \frac{2}{\gamma - 1}\left[\left(1 + \frac{\gamma - 1}{2} M_e^2\right)\left(\frac{p_t}{p_{t,e}}\right)^{\frac{\gamma-1}{\gamma}} - 1\right] \qquad (13)$$

9

The temperature and velocity profiles are assumed to be related by the Crocco-Busemann relation (ref. 20, p. 627)

$$T \approx T_w + (T_{aw} - T_w)\frac{u}{u_e} - \frac{ru^2}{2c_p} \tag{14}$$

For the case of an adiabatic-wall condition, equation (14) can be written as

$$\frac{T}{T_e} = 1 + r\frac{\gamma - 1}{2} M_e^2 \left[1 - \left(\frac{u}{u_e}\right)^2\right] \tag{15a}$$

The temperature is related to the local Mach number and velocity by

$$\frac{T}{T_e} = \left(\frac{u}{u_e}\frac{M_e}{M}\right)^2 \tag{15b}$$

By using equations (13) and (15), the velocity profile can be expressed in terms of the Mach number as

$$\frac{u}{u_e} = \frac{M}{M_e}\left(\frac{1 + r\frac{\gamma - 1}{2}M_e^2}{1 + r\frac{\gamma - 1}{2}M^2}\right)^{1/2} \tag{16}$$

By knowing the velocity distribution and the density distribution given by the Crocco-Busemann relation, the boundary-layer integral parameters can be evaluated. For the region between the wall and the first tube ($y/\delta \approx 0.05$), an analytical approximation corresponding to a suitable power-law profile was used.

RESULTS AND DISCUSSION

Boundary Layer Without Suction

The first objective in the current investigation was to analyze the solid-wall boundary-layer data to obtain an estimate of the boundary-layer integral parameters (δ^*, θ, and H) under various operating conditions. These values were used to establish base-line boundary-layer properties that were later compared with the boundary-layer properties with suction. For this purpose, the measurements made by the pitot rake located ahead of the suction region are considered. By knowing the boundary-layer parameters at this station, the values at the model location can be estimated by using standard boundary-layer prediction methods.

Figure 6 shows a typical variation of total pressure, Mach number, and velocity within the boundary layer for a test-section Mach number of 0.76 and a Reynolds number of 40×10^6 per meter. Detailed velocity profiles under different conditions of operation and with zero boundary-layer suction are presented in figure 7. It may be noted that the boundary-layer velocity profiles ahead of the perforated plate on two sidewalls agree closely. The integral parameters evaluated by using these profiles are shown in figure 8. The error bounds shown indicate the uncertainty in the measured values. The displacement and momentum thicknesses show a slight reduction with increase in unit Reynolds number. At the lowest Reynolds number tested of 20×10^6 per meter, δ^* and θ are, respectively, about 1.7 and 1.3 mm and decrease to about 1.3 and 0.9 mm at the highest Reynolds number of 200×10^6 per meter. The shape parameter is seen to increase from 1.3 at $M = 0.30$ to about 1.5 at $M = 0.76$, and the effect of Reynolds number over the range tested (from 20 to 200×10^6 per meter) was not significant.

The mean velocity profiles have been correlated in figure 9 over the range of Mach number and Reynolds number of these tests. Most of the data points from the profiles fall in the outer region of the turbulent boundary layer (i.e., $y/\delta > 0.15$) and show good agreement with the defect law of Hama (ref. 21, p. 631):

$$\frac{u_e - u}{u_\tau} = 9.6 \left(1 - \frac{y}{\delta} \right)^2 \tag{17}$$

The data in figure 9 were correlated in terms of y/δ^*, rather than of y/δ (eq. (17)), to avoid uncertainties in properly locating the outer edge of the boundary layer. The modification of equation (17) was also used in reference 22 where $\delta = 8\delta^*$ was found to give a good correlation at low Reynolds numbers where the power-law velocity-profile exponent is near the 1/N-power law. The N-power relationship used in equation (17) and figure 9 to relate δ and δ^* varies with Reynolds number, as indicated in reference 23. For instance, at a low Reynolds number the power-law velocity-profile exponent is nearer 1/7 and, thus, $\delta = 8\delta^*$. However, at the higher Reynolds numbers of these tests, the exponent increases and $\delta = 9\delta^*$ and $\delta = 10\delta^*$ were used in equation (17). The friction velocity u_τ was calculated by using the local skin-friction values from equation (4) and the corresponding values of R_θ and H. It may be seen from figure 9 that the measured velocity profiles correlate well with equation (17), with $\delta = 9\delta^*$ at $R = 40 \times 10^6$ per meter and with $\delta = 10\delta^*$ at $R = 170 \times 10^6$ per meter.

The velocity profiles (fig. 7) measured by the rakes located downstream of the perforated plates are affected by the boundary-layer growth over the plate even when there is no suction. The characteristics of the boundary layer over a porous surface are quite complicated, depending on the nature of the porous media used. Recent studies by Schetz and Kong (refs. 22 and 24) show that the surface porosity and surface roughness tend to lower the intercept of the logarithmic portion of the wall law and to cause a significant increase in skin friction and turbulence quantities.

Even though the scope of the present investigation was not adequate to probe the inner region in detail, the change in the integral parameters across the perforated plate can be expected to give some idea of the severity of the boundary-layer growth over the perforated plate with closely spaced holes. The increase in momentum thickness across the perforated plate under zero mass-flow removal conditions is shown in figure 10. It may be observed that on one of the walls (SW1), the increase in momentum thickness is much higher than on the other wall. The presence of a small step at the junction of the wall and of the perforated plate on this wall, which was

noticed later, might possibly have caused this increase. Since the perforated-plate surface exposed to flow is finished to a high degree of smoothness, it is likely that the surface-roughness effects may not be very significant. However, the discrete-hole configuration to some extent may give rise to an open-area effect with free-jet-type mixing resulting in a higher growth rate of the boundary layer than on a solid wall. A simple estimate of the boundary-layer growth expected with free-jet-type mixing along the open area is given by (ref. 10)

$$\frac{\Delta \delta^*}{L} = 0.01023 (\bar{R})^{2/3} \quad \text{or} \quad \frac{\Delta \theta}{L} \approx 0.0073 (\bar{R})^{2/3} \qquad (\text{for} \quad H = 1.4) \qquad (18)$$

The present tests indicated that with no suction the increase in momentum thickness is between 0.1 and 0.3 mm with the majority of data being between 0.1 and 0.2 mm. These values are well within the estimates of equation (18), which can be expected to give an upper bound on the shear-layer growth. An earlier investigation (ref. 5) in the 0.3-m TCT, with a perforated plate of 24-percent porosity with 0.46-mm-diameter holes and 0.82-mm spacing, indicated that with no suction there was a significant increase in momentum thickness across the plate, possibly because of the larger holes and surface roughness. These previous results from reference 5 indicated that perforated plates would require considerably more suction to overcome the adverse growth of the boundary layer before the benefits of suction can be realized. The measurements presented herein suggest that when the current technique for the manufacture of perforated plates (i.e., smaller holes) is used, the growth of the boundary layer in the absence of suction is not significant and this type of porous media may be superior to other types using sintered woven screen materials. A more detailed investigation of the turbulent boundary-layer development with emphasis on the inner region is desirable to evaluate the merits of the perforated-plate suction medium having hole diameter and spacing much less than the boundary-layer thickness.

Effect of Boundary-Layer Suction

The effect of the boundary-layer bleed on velocity profiles is shown in figure 11 for $M = 0.76$ and $R = 40 \times 10^6$ per meter. Highest bleed rates of up to 2.4 percent were obtained for this test condition with passive boundary-layer bleed operation. Also, at this Mach number, the differences in boundary-layer growth without suction on two sidewalls were most pronounced. It may be observed that even with small bleed rates the velocity profiles tend to become fuller and the differences between the two walls diminish. With about 1-percent bleed rate, the profiles almost overlap, which indicates good uniformity of the flow on both sidewalls downstream of the suction region. With further increase in bleed rate, the change in velocity profiles is rather slower and, after about 2-percent bleed rate, the suction seems to have little effect. Such behavior is to be expected because of the increase in skin friction with suction which tends to neutralize the beneficial effect of suction. The extent of thinning down of the boundary layer with increase in suction is also apparent from the velocity profiles. The velocity at the first tube located 0.6 mm away from the wall increases from about $0.7u_e$ with no suction to about $0.87u_e$ with suction. Figures 12 and 13 show the velocity profiles for different Reynolds numbers and Mach numbers, respectively, with 1-percent boundary-layer bleed. No significant change in the velocity profiles is noted in the test range because of the dominant effect of suction on skin friction compared with changes with Reynolds number and Mach number.

The change in momentum thickness ($\Delta\theta$) across the perforated plate with suction is shown for different Reynolds numbers and Mach numbers in figures 14 and 15, respectively. The measured increase in the absence of suction is about 0.3 mm. With application of suction, the boundary layer thins down rapidly, and for about 0.5-percent bleed, the suction is sufficient to overcome the increase in the boundary-layer growth over the perforated plate when there is no suction. With a further increase, the boundary layer thins down gradually, and after about 1-percent bleed, the effectiveness decreases considerably. As discussed earlier, with over 2-percent bleed the change in momentum thickness is negligible. The loss in effectiveness of suction at higher bleed rates suggests that with the suction arrangement employed for the 0.3-m TCT, the useful range of boundary-layer bleed is limited to about 2 percent (1 percent for each wall), above which only a drop in test-section Mach number will occur without any appreciable thinning of the boundary layer.

Comparison With Theoretical Predictions

Theoretical calculations of the boundary-layer growth with suction have been made for the case of $M = 0.76$ and $R = 40 \times 10^6$ per meter. Since a finite quantity of mass is removed from the test-section flow through boundary-layer suction, a positive pressure gradient is established along the flow direction across the suction region. This adverse pressure gradient results in a Mach number drop and also tends to diminish the effectiveness of suction. For small mass-flow removal rates, as in the present case, this effect is small. Figure 16 shows the measured change in Mach number with bleed for an upstream Mach number of 0.76. For the boundary-layer calculations, a linear approximation to this measured data was used.

For the finite-difference method (refs. 12 and 13), the initial step size in the y-direction was reduced with an increase in bleed rate in order to have at least four steps in the linear region. The number of steps in the y-direction varied from about 250 with no bleed to 300 with 2.4-percent bleed. For the highest bleed rate, step sizes in the x-direction of 0.7 and 0.14 mm were tried, and it was determined that the final integral parameters differed very little; therefore, for all other conditions, the larger step size was used.

A comparison between the measured $\Delta\theta$ and the predictions of the finite-difference and integral methods is shown in figure 17. Both methods predict the proper trend in the effectiveness of suction to the maximum bleed rate of 2.4 percent, corresponding to $v_w/u_e \approx -0.02$. The results of the finite-difference method are closer to the data, and the integral approach tends to underpredict the decrease in $\Delta\theta$ somewhat. The initial increase in momentum thickness with zero suction is approximately the same as would be expected on a solid wall. This result further suggests that there is no significant adverse growth over the perforated plates when there is no suction. A comparison of the change in the measured shape parameter with predictions, shown in figure 18, is satisfactory with the two theories bracketing the data. However, the finite-difference method predicts the trend in H better than the integral method.

Good agreement is shown in figure 19 between measured velocity profiles with suction and the results of the finite-difference calculation. Both the data and theory show the characteristic thinning of the boundary layer with increasing suction, as well as higher values of u/u_e as the suction increases. The reasonable agreement of the predictions with the measurements demonstrates the adequacy of the

13

calculation methods in providing good estimates of the boundary-layer properties with suction through perforated plates with closely spaced holes, even for high bleed rates.

With limited measurements on a single perforated plate, it is difficult to say whether some differences between the measurements and theory are due to discrete-suction effects or otherwise. In an effort to examine this question, calculations were made with a code developed by Streett (ref. 5) to account for the discrete suction in an indirect manner. The results, using the method of Streett, were close to the predictions of the integral method for low bleed rates. However, when Streett's method was used with increasing bleed rates, the boundary-layer thickness started increasing rapidly rather than thinning, probably because of overcorrection for discrete-suction effects. These results substantiated that the previously dis-cussed assumption of continuous suction averaged over the surface (eq. (1)) is reasonable and that the inviscid-sink effects are not significant for these tests.

Even though the predictions of the finite-difference calculation are closer to the data than to the integral methods, a simpler approach, based on integral methods, is desirable for quick estimates and rapid calculation. In order to have a rapid integral method, a simple skin-friction relation accounting for suction is needed. The basis for this type of skin friction is found in reference 25 where the skin friction with suction is related to the value without suction $C_{f,0}$ by

$$ C_f = -K \frac{\rho_w v_w}{\rho_e u_e} \bigg/ \left[1 - \exp\left(\frac{K}{C_{f,0}} \frac{\rho_w v_w}{\rho_e u_e} \right) \right] \tag{19} $$

with $K = 1.62$. The constant 1.62 from reference 25 was based on data obtained over a limited range of boundary-layer bleed. For the higher bleed rates pertinent to this study, the skin friction increases linearly with suction velocity, which is indicated in equation (19), since the denominator approaches unity rapidly. A com-parison of the values of C_f obtained by using equation (19) with the detailed charts of reference 16 indicated that the two agree for large Reynolds numbers and for $H = 1.2$. The skin-friction relation given in equation (19) can be used in conjunction with the following Von Kármán momentum integral relation to make rapid calculations:

$$ \frac{d\theta}{dx} + \frac{\theta}{u_e} \frac{du_e}{dx} \left(2 + H - M_e^2 \right) = \frac{\tau_w}{\rho_e u_e^2} + \frac{\rho_w v_w}{\rho_e u_e} \tag{20} $$

The last terms on the two sides of equation (20) account for the pressure gradient and mass-transfer effects, respectively. When the velocity-gradient term is modified and the assumption of a uniformly distributed suction is made, the change in momentum thickness across the porous plate can be expressed as

$$ \Delta\theta = \left(\frac{C_f}{2} + \frac{\rho_w v_w}{\rho_e u_e} \right)L - \frac{\theta\left(2 + H - M_e^2\right)}{1 + 2M_e^2} \frac{\Delta M}{M_e} \tag{21} $$

14

A comparison of $\Delta\theta$ is made in figure 20 between experimental data and predictions using equations (19) and (21). The agreement between the data and theory was quite good when $K = 1.4$ was used instead of $K = 1.62$. This suggests that a simple integral relationship coupled with an appropriate skin-friction expression can be used to make quick and reasonably accurate estimates of the change in boundary-layer properties due to suction across a perforated plate with closely spaced holes. For high suction rates and zero-pressure-gradient flows, equation (21) simplifies to

$$\Delta\theta = \left(1 - \frac{K}{2}\right)\frac{\rho_w v_w}{\rho_e u_e} L \tag{22}$$

CONCLUSIONS

An experimental and theoretical study of the sidewall boundary layer was conducted in the Langley 0.3-Meter Transonic Cryogenic Tunnel by using the recently incorporated boundary-layer control system. The study was focused on an evaluation of the effectiveness of the boundary-layer suction in terms of the change in boundary-layer properties across the porous plate over a range of operating conditions. The results of the study indicated the following conclusions:

1. The displacement thickness on the test-section sidewall (about 0.3 m upstream of the airfoil location) varies from 1.6 to 1.3 mm at unit Reynolds numbers from 20 to 200 × 10^6 per meter, respectively. The shape parameter increases from about 1.3 at a low Mach number M of 0.30 to about 1.5 at $M = 0.76$.

2. The sidewall velocity profiles in the outer region correlate well with the defect law of Hama.

3. When there was no suction, the perforated plates with closely spaced holes indicated little adverse growth of the boundary layer.

4. At $M = 0.76$ with suction applied to the boundary layer, the displacement thickness and the momentum thickness downstream of the perforated plate decrease for suction levels as high as 2.4 percent of the test-section mass flow. However, the rate of decrease gets smaller as suction increases from 0 to 2.4 percent.

5. The effect of Mach number and Reynolds number on the boundary-layer properties over the range of conditions tested was small compared with the effect of suction.

6. A comparison of the change in boundary-layer properties resulting from suction with the predictions of finite-difference and integral methods showed good agreement. The results indicated that these two methods can be used to obtain estimates of the boundary-layer growth with suction over perforated plates with hole diameter and spacing much less than the local boundary-layer thickness. The results of finite-difference calculations agreed better with the data than the results of the integral method; however, both methods showed the correct trend with increasing suction to free-stream velocity ratios as high as -0.02.

7. The good agreement between data and theories suggests that the inviscid-sink effect due to discrete perforations for the hole sizes used in these tests is not significant and, therefore, the assumption of continuous suction is reasonable.

8. The Von Kármán momentum integral equation coupled with a simplified skin-friction expression can be used to obtain reasonable estimates of boundary-layer changes across a perforated plate with suction.

Langley Research Center
National Aeronautics and Space Administration
Hampton, VA 23665
November 30, 1982

REFERENCES

1. Kilgore, Robert A.: Design Features and Operational Characteristics of the Langley 0.3-Meter Transonic Cryogenic Tunnel. NASA TN D-8304, 1976.

2. Goodyer, Michael J.: The Self Streamlining Wind Tunnel. NASA TM X-72699, 1975.

3. Barnwell, Richard W.: A Similarity Rule for Compressibility and Sidewall-Boundary-Layer Effects in Two-Dimensional Wind Tunnels. AIAA Paper 79-0108, Jan. 1979.

4. Sewall, W. G.: The Effects of Sidewall Boundary Layers in Two-Dimensional Subsonic and Transonic Wind Tunnels. AIAA-81-1297, June 1981.

5. Streett, Craig Leroy: A Method for Computing Boundary Layer Growth on a Perforated Suction Surface. M.S. Thesis, The George Washington Univ., May 6, 1979.

6. Ray, Edward J.; Ladson, Charles L.; Adcock, Jerry B.; Lawing, Pierce L.; and Hall, Robert M.: Review of Design and Operational Characteristics of the 0.3-Meter Transonic Cryogenic Tunnel. NASA TM-80123, 1979.

7. Thibodeaux, Jerry J.; and Balakrishna, S.: Development and Validation of a Hybrid-Computer Simulator for a Transonic Cryogenic Wind Tunnel. NASA TP-1695, 1980.

8. Kilgore, Robert A.: Model Design and Instrumentation Experiences With Continuous-Flow Cryogenic Tunnels. Cryogenic Wind Tunnels, AGARD-LS-111, May 1980, pp. 9-1 - 9-22.

9. Kilgore, Robert A.: Selection and Application of Instrumentation for Calibration and Control of a Continuous-Flow Cryogenic Tunnel. Cryogenic Wind Tunnels, AGARD-LS-111, May 1980, pp. 11-1 - 11-10.

10. Goethert, Bernhard H.: Transonic Wind Tunnel Testing. AGARDograph No. 49, Pergamon Press, 1961.

11. Wuest, W.: Survey of Calculation Methods of Laminar Boundary Layers With Suction in Incompressible Flow. Boundary Layer and Flow Control - Its Principles and Application, Volume 2, G. V. Lachmann, ed., Pergamon Press, Ltd., 1961, pp. 771-800.

12. Hixon, Barbara A.; Beckwith, Ivan E.; and Bushnell, Dennis M.: Computer Program for Compressible Laminar or Turbulent Nonsimilar Boundary Layers. NASA TM X-2140, 1971.

13. Bushnell, Dennis M.; and Beckwith, Ivan E.: Calculation of Nonequilibrium Hypersonic Turbulent Boundary Layers and Comparisons With Experimental Data. AIAA J., vol. 8, no. 8, Aug. 1970, pp. 1462-1469.

14. Adcock, Jerry B.; and Johnson, Charles B.: A Theoretical Analysis of Simulated Transonic Boundary Layers in Cryogenic-Nitrogen Wind Tunnels. NASA TP-1631, 1980.

15. Cebeci, Tuncer: Behavior of Turbulent Flow Near a Porous Wall With Pressure Gradient. AIAA J., vol. 8, no. 12, Dec. 1970, pp. 2152-2156.

16. Thompson, B. G. J.: A Three-Parameter Family of Mean Velocity Profiles for Incompressible Turbulent Boundary Layers With Distributed Suction and Small Pressure Gradient. R. & M. No. 3622, British A.R.C., 1970.

17. Lin, C. C., ed.: Turbulent Flows and Heat Transfer. Princeton Univ. Press, 1959.

18. Towne, Charles E.: Evaluation of Analytical Procedures for Prediction of Turbulent Boundary Layers on a Porous Wall. NASA TM X-3063, 1974.

19. Sasman, Philip K.; and Cresci, Robert J.: Compressible Turbulent Boundary Layer With Pressure Gradient and Heat Transfer. AIAA J., vol. 4, no. 1, Jan. 1966, pp. 19-25.

20. White, Frank M.: Vicsous Fluid Flow. McGraw-Hill, Inc., c.1974.

21. Hinze, J. O.: Turbulence, Second ed. McGraw-Hill Book Co., c.1975.

22. Kong, Fred Y.; and Schetz, Joseph A.: Turbulent Boundary Layer Over Solid and Porous Surfaces With Small Roughness. AIAA-81-0418, Jan. 1981.

23. Johnson, Charles B.; and Bushnell, Dennis M.: Power-Law Velocity-Profile-Exponent Variations With Reynolds Number, Wall Cooling, and Mach Number in a Turbulent Boundary Layer. NASA TN D-5753, 1970.

24. Kong, Fred Y.; and Schetz, Joseph A.: Turbulent Boundary Layer Over Porous Surfaces With Different Surface Geometries. AIAA-82-0030, Jan. 1982.

25. Verollet, E.; Fulachier, L.; Dumas, R.; and Favre, A.: Turbulent Boundary Layer With Suction and Heating to the Wall. Heat and Mass Transfer in Boundary Layers - Volume 1, N. Afgan, Z. Zaric, and P. Anastasijevic, eds., Pergamon Press, Inc., c.1972, pp. 157-168.
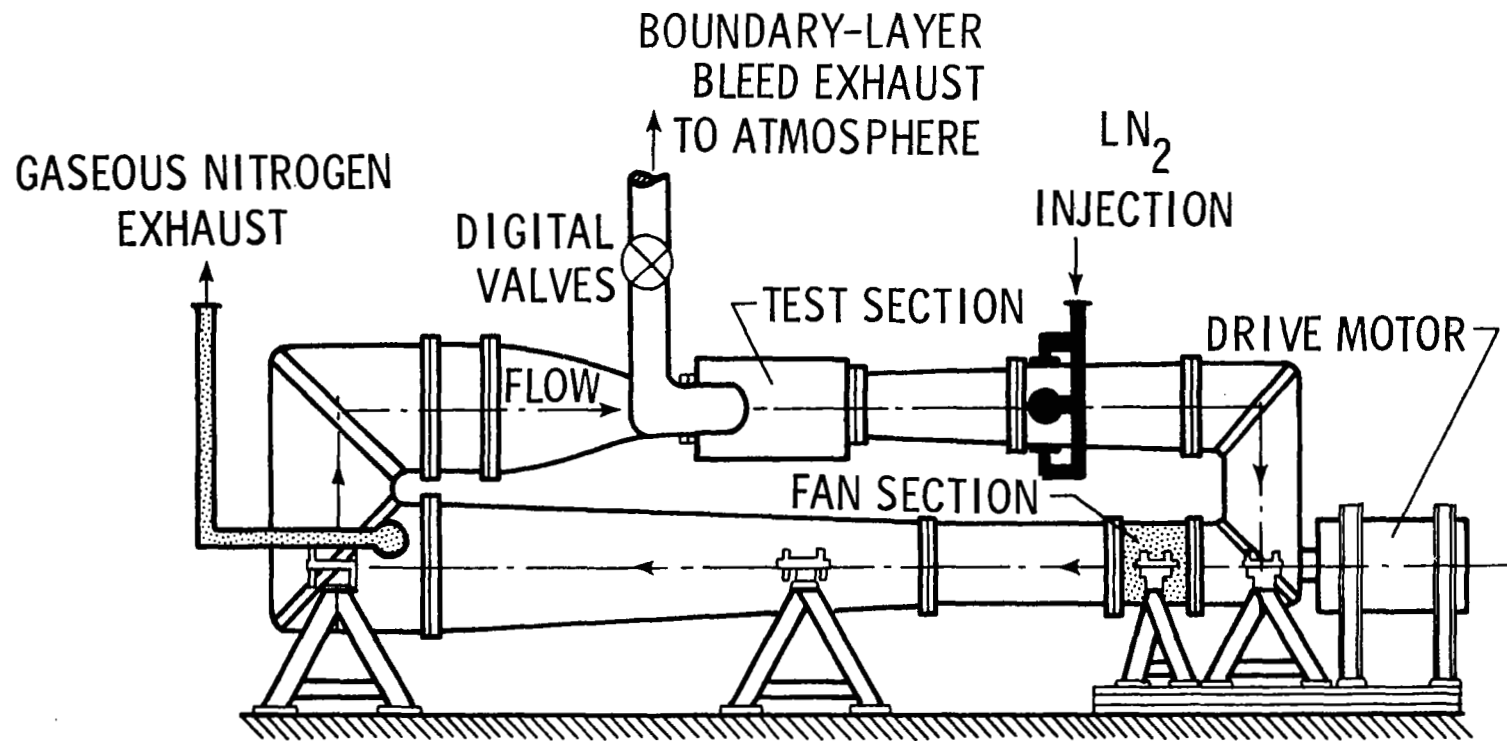
Figure 1.- Schematic drawing of the Langley 0.3-Meter Transonic Cryogenic Tunnel (0.3-m TCT).
M = 0 to 0.95; p_t = 1.2 to 6 atm; T_t, condensation limit to 320 K.
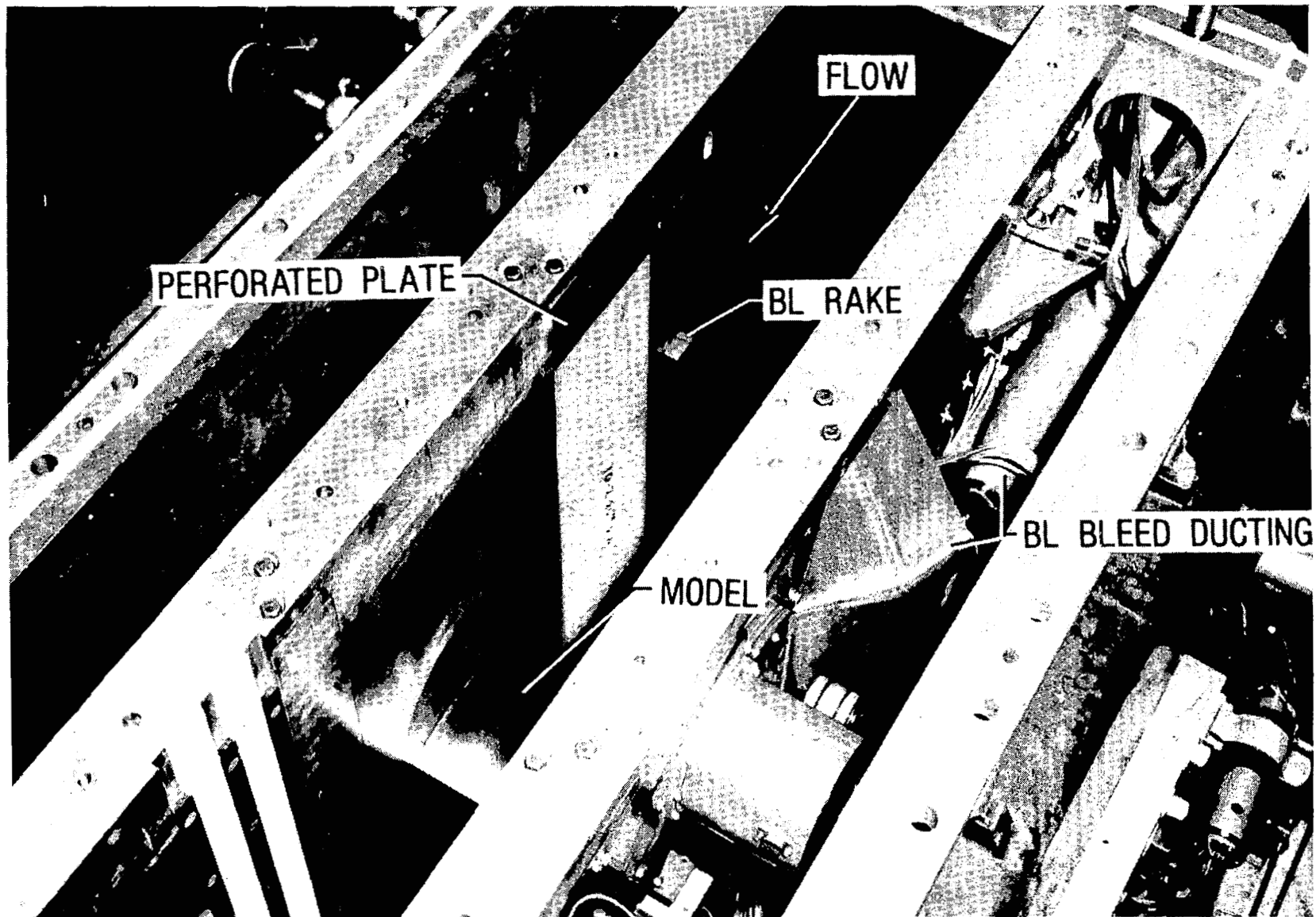
L-82-210

Figure 2.- Photograph of two-dimensional test section of the Langley 0.3-m TCT with perforated plates for suction. Model was not in test section for the present study.
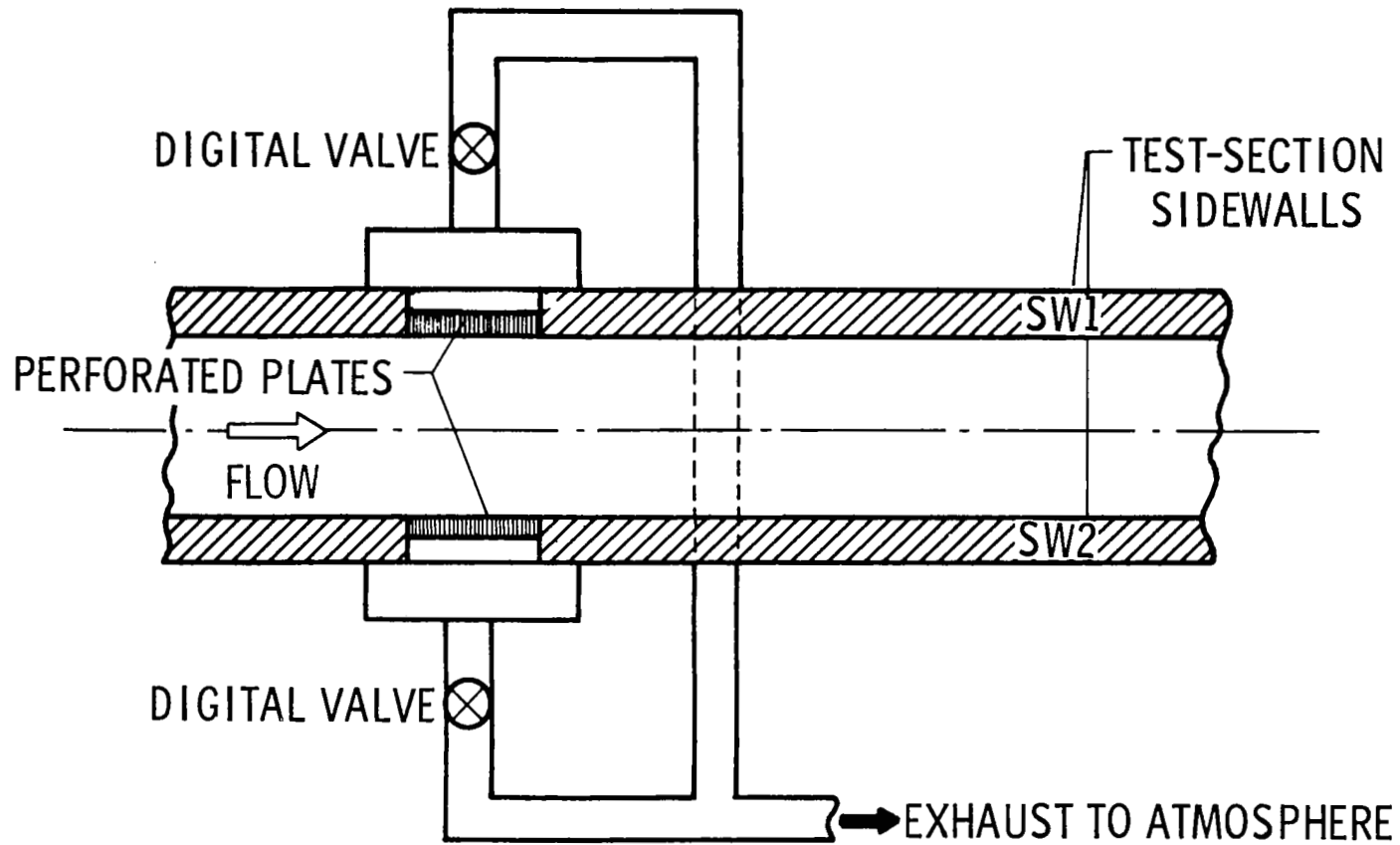
Figure 3.- Schematic drawing of sidewall boundary-layer removal system with passive bleed.
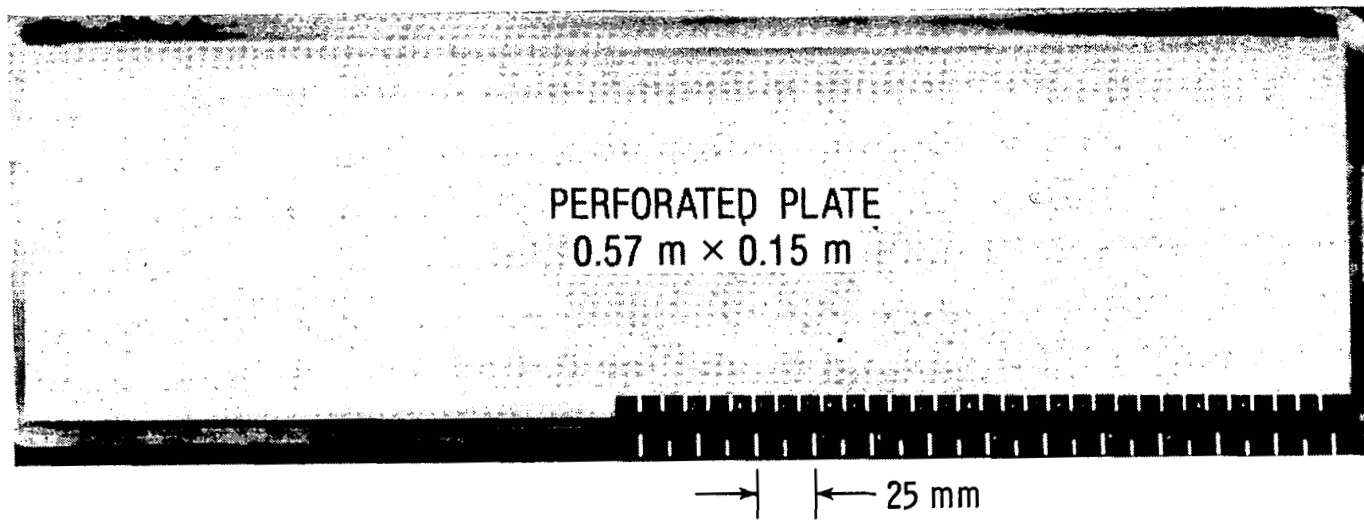
(a) Full plate.
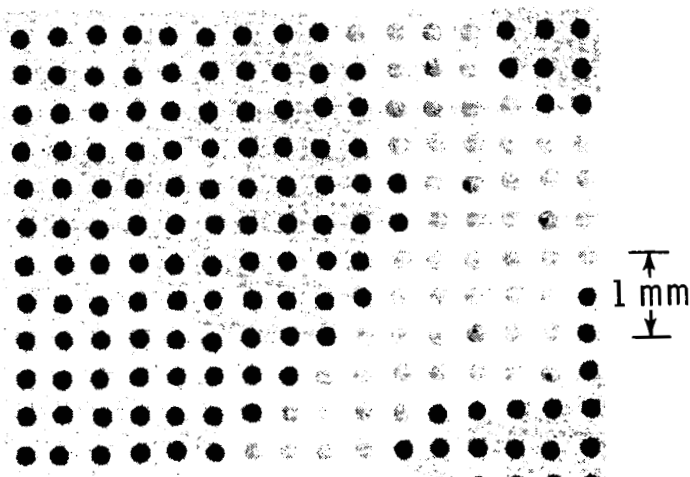
(b) Approximate magnification, ×11.
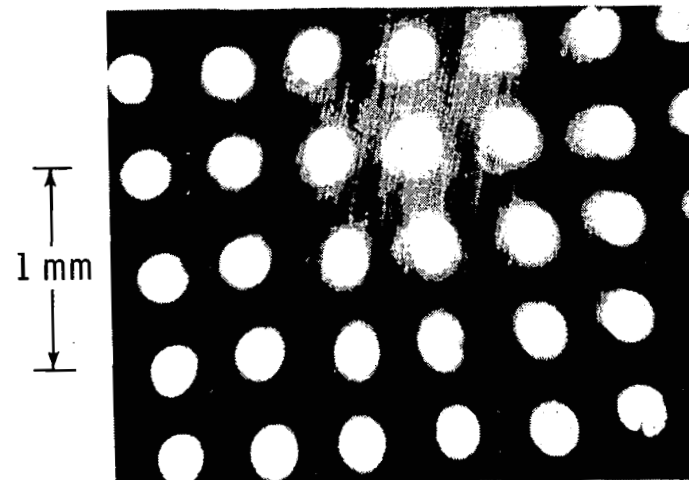
(c) Approximate magnification, ×30.

L-82-211

Figure 4.- Electron beam-drilled perforated plate used for boundary-layer suction.

FLOW →

387.4

114.3

215.9

228.6 DIAM.

AIRFOIL
TURNTABLE
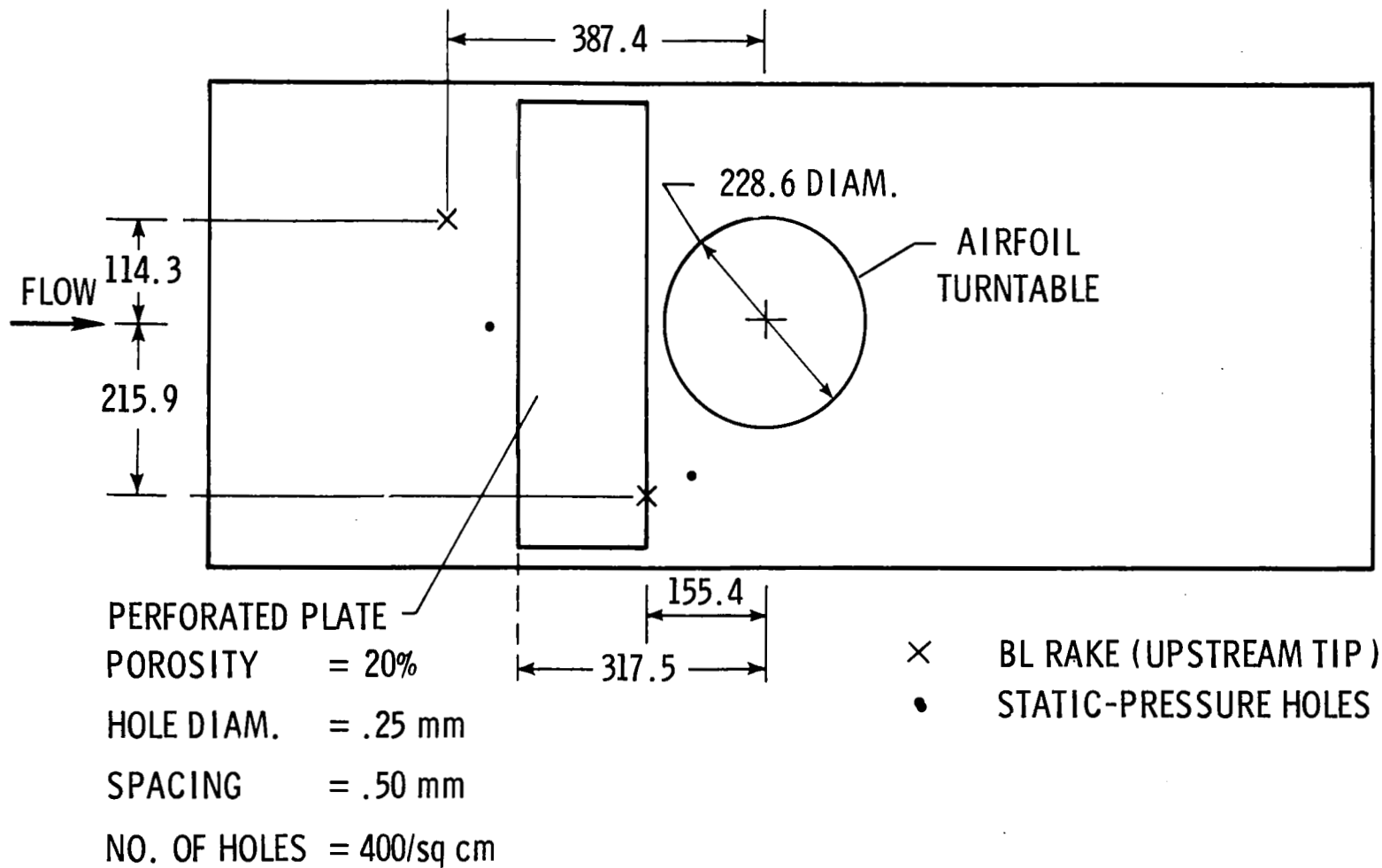
PERFORATED PLATE
POROSITY   = 20%
HOLE DIAM.   = .25 mm
SPACING   = .50 mm
NO. OF HOLES = 400/sq cm

155.4

317.5

× BL RAKE (UPSTREAM TIP)
• STATIC-PRESSURE HOLES

(a) Measurement stations on right test-section sidewall (SW1).

Figure 5.- Sidewall measurements. Dimensions are given in millimeters unless otherwise specified.
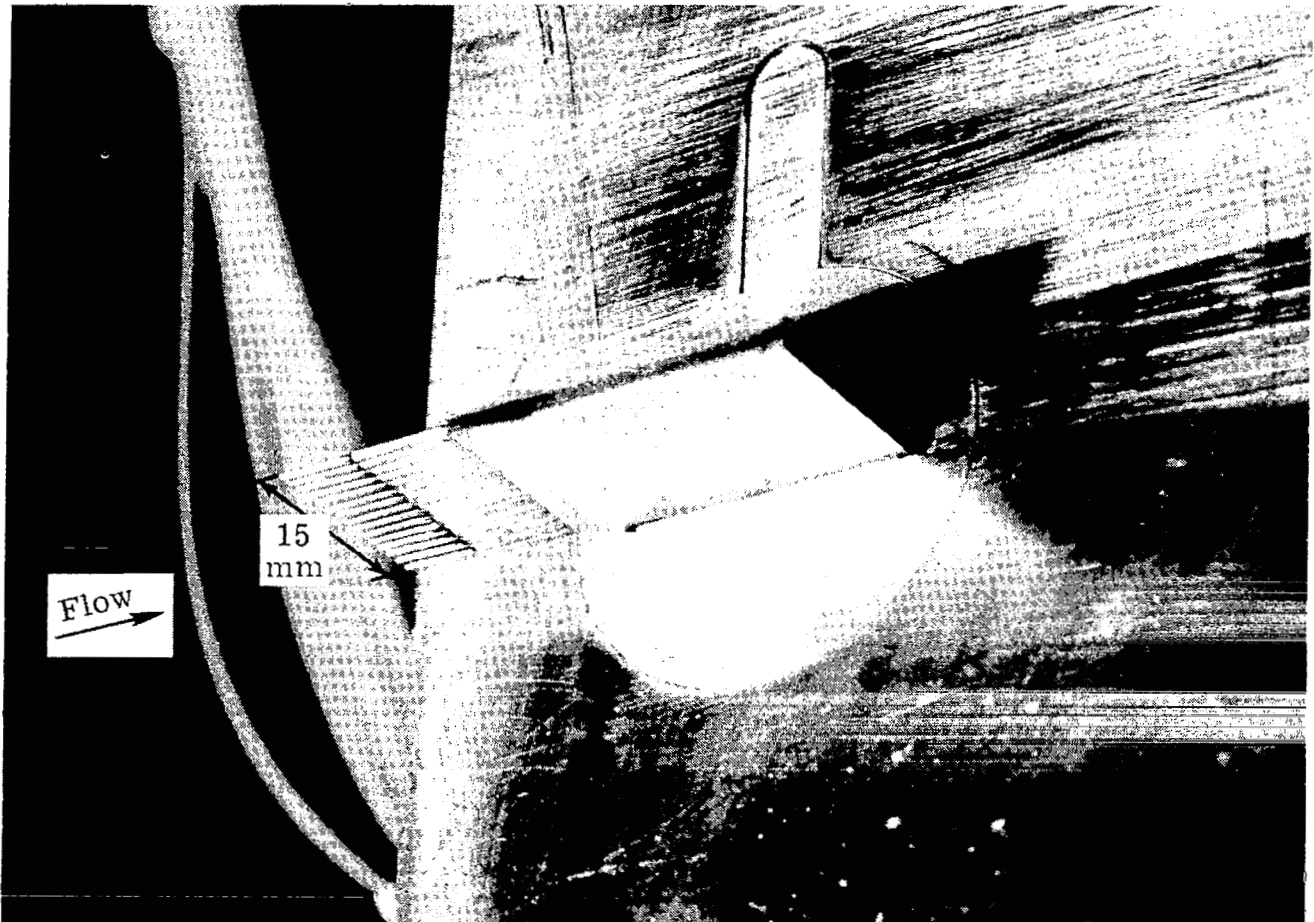
L-82-8981.1

(b) Photograph of sidewall boundary-layer rake. Probe outside diameter, 0.5 mm; wall thickness, 0.125 mm.

Figure 5.- Concluded.
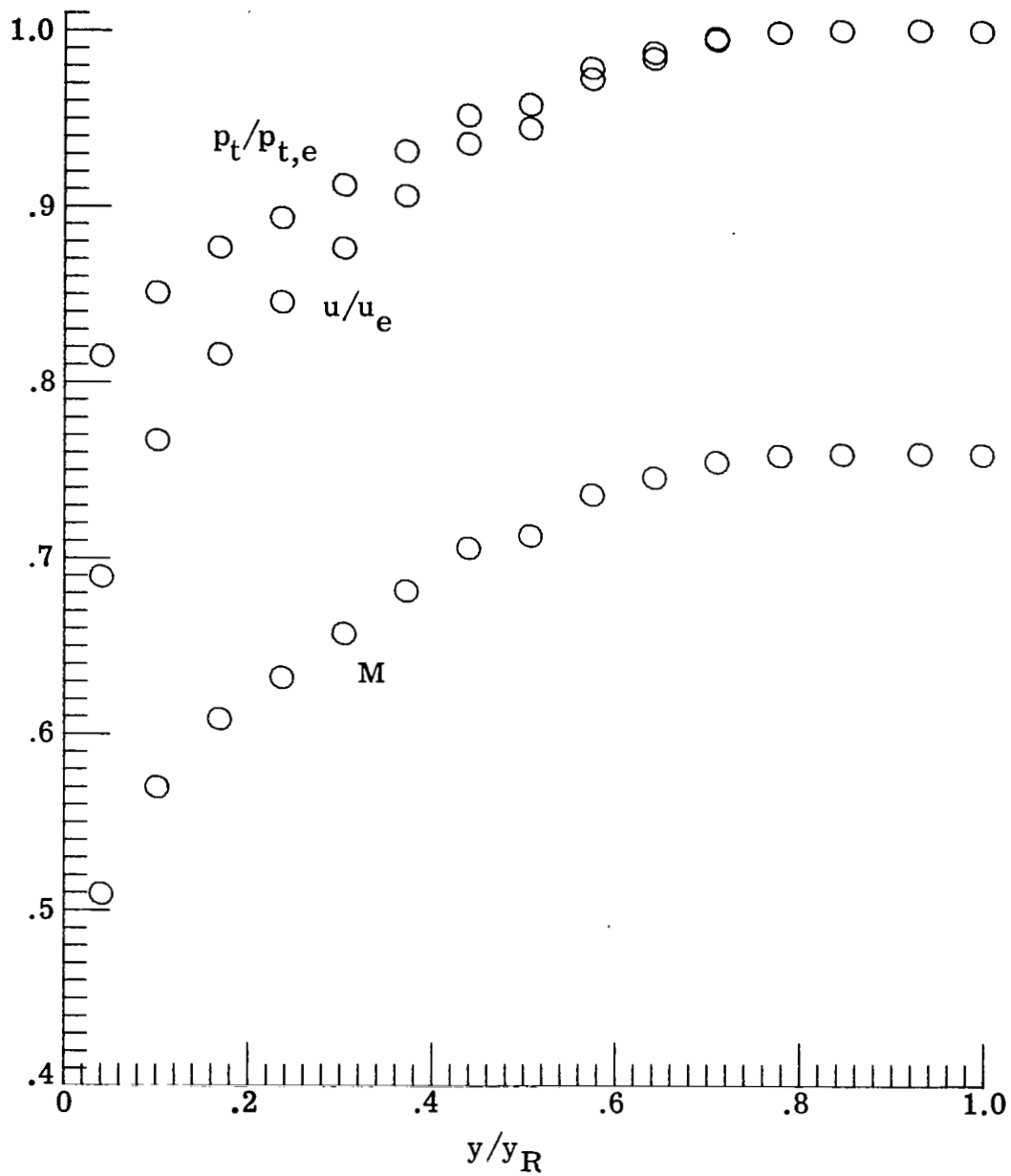
Figure 6.– Typical experimental sidewall boundary-layer profiles of total pressure, Mach number, and velocity upstream of perforated plate. $y_R = 15$ mm; $M = 0.76$; $R = 40 \times 10^6$ per meter.
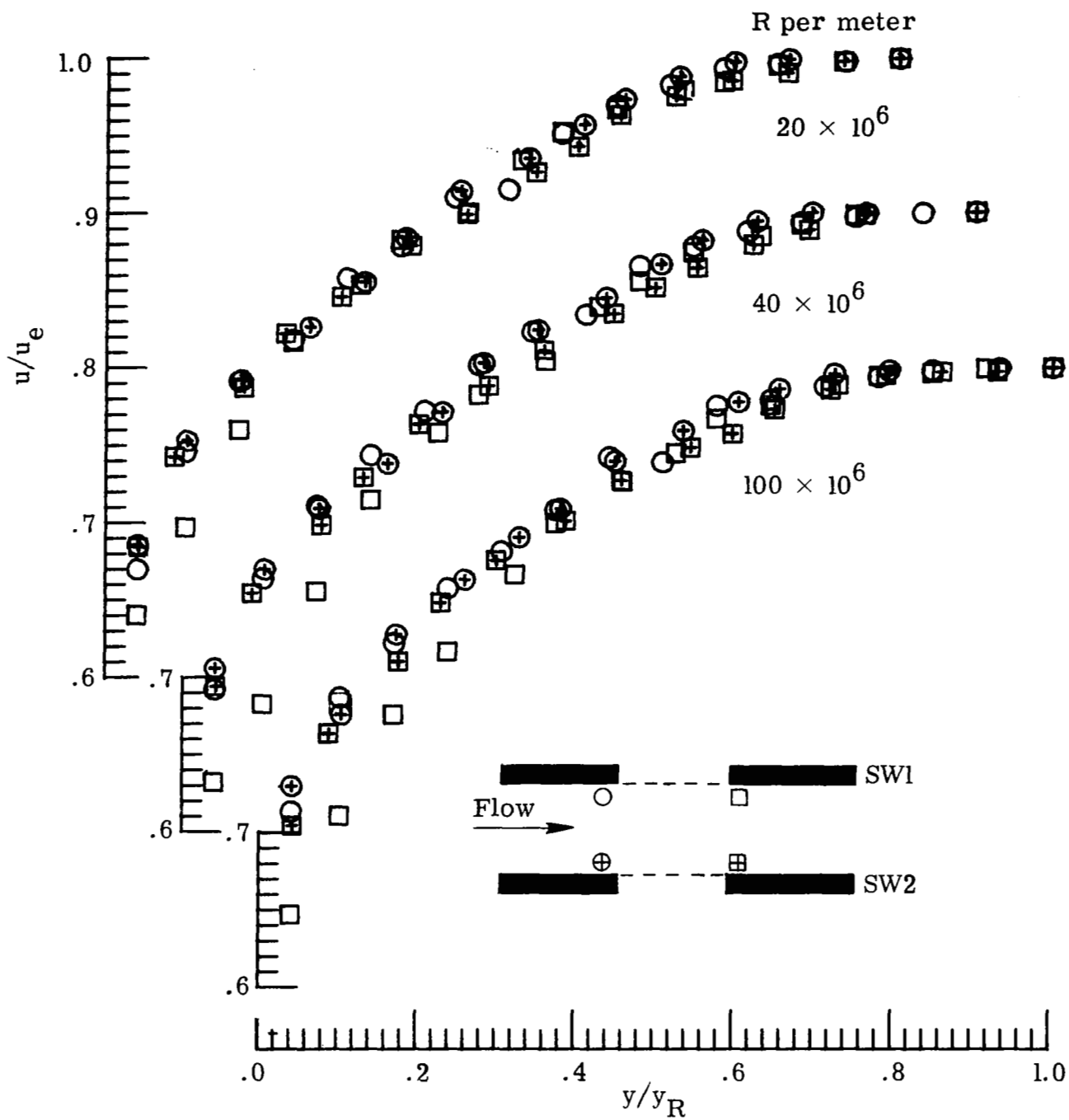
(a) M = 0.30.

Figure 7.- Velocity profiles ahead and behind perforated plate with no suction. y_R = 15 mm.
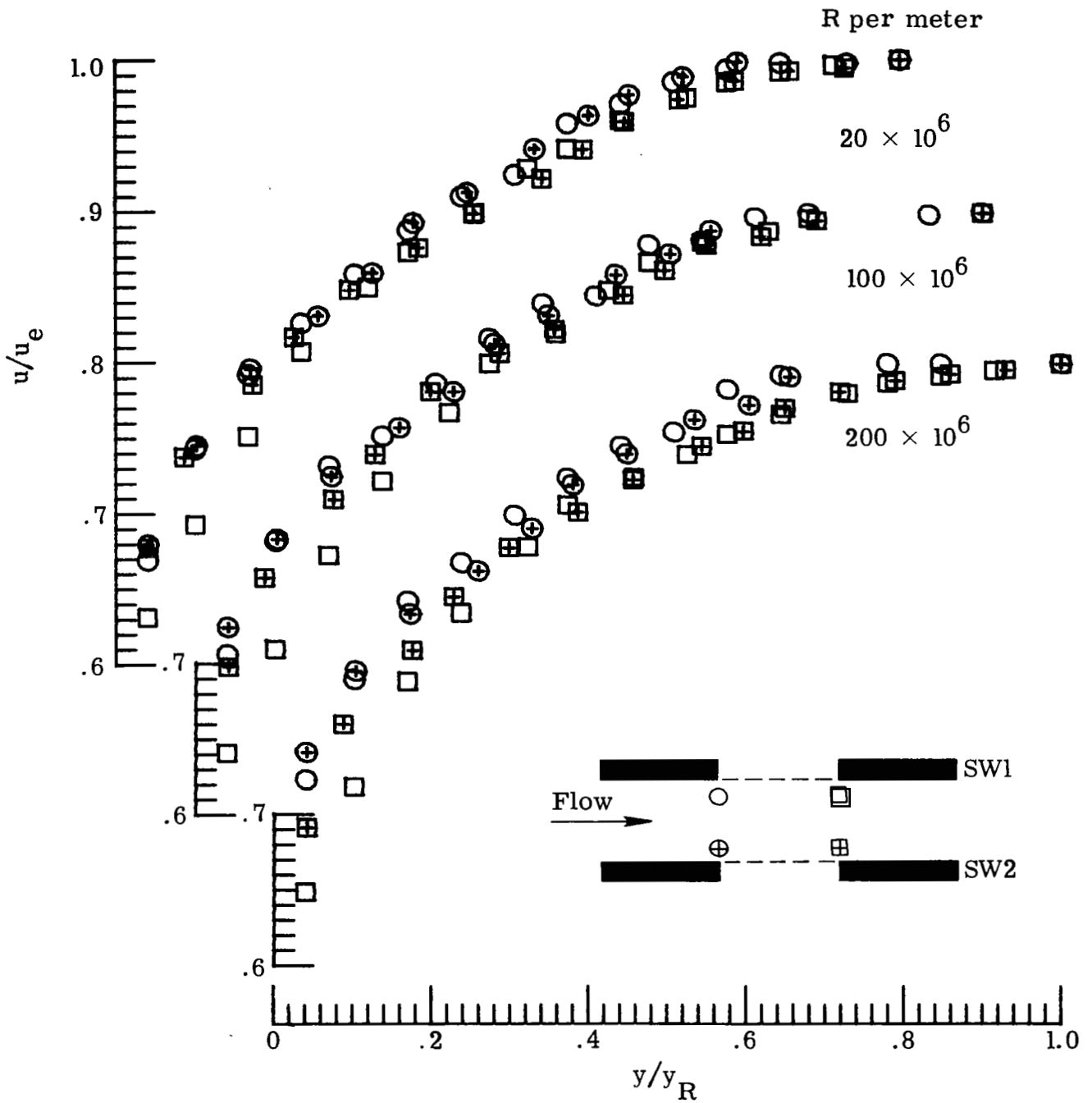
(b)   M = 0.50.

Figure 7.- Continued.
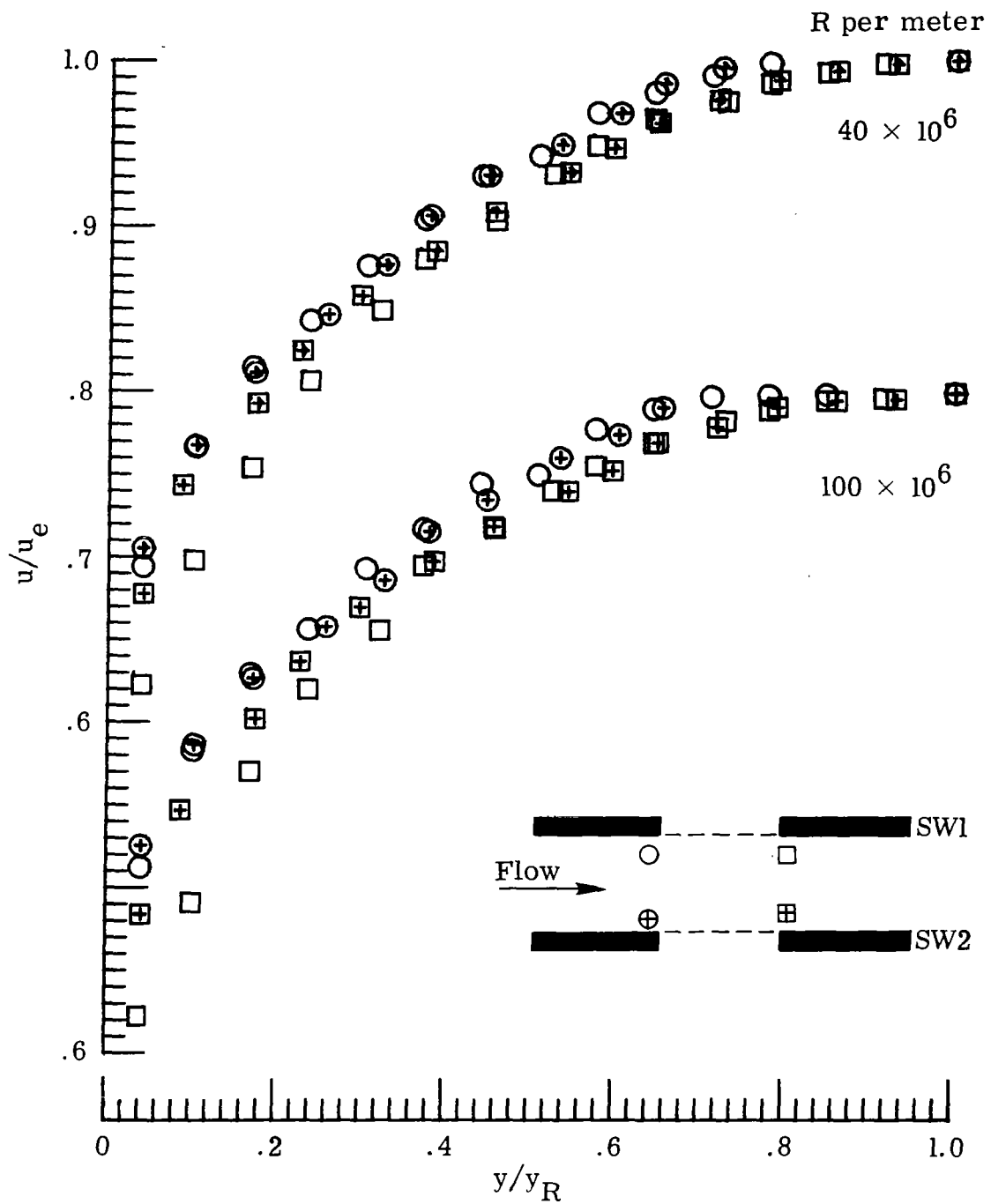
(c)   M = 0.60.

Figure 7.- Continued.
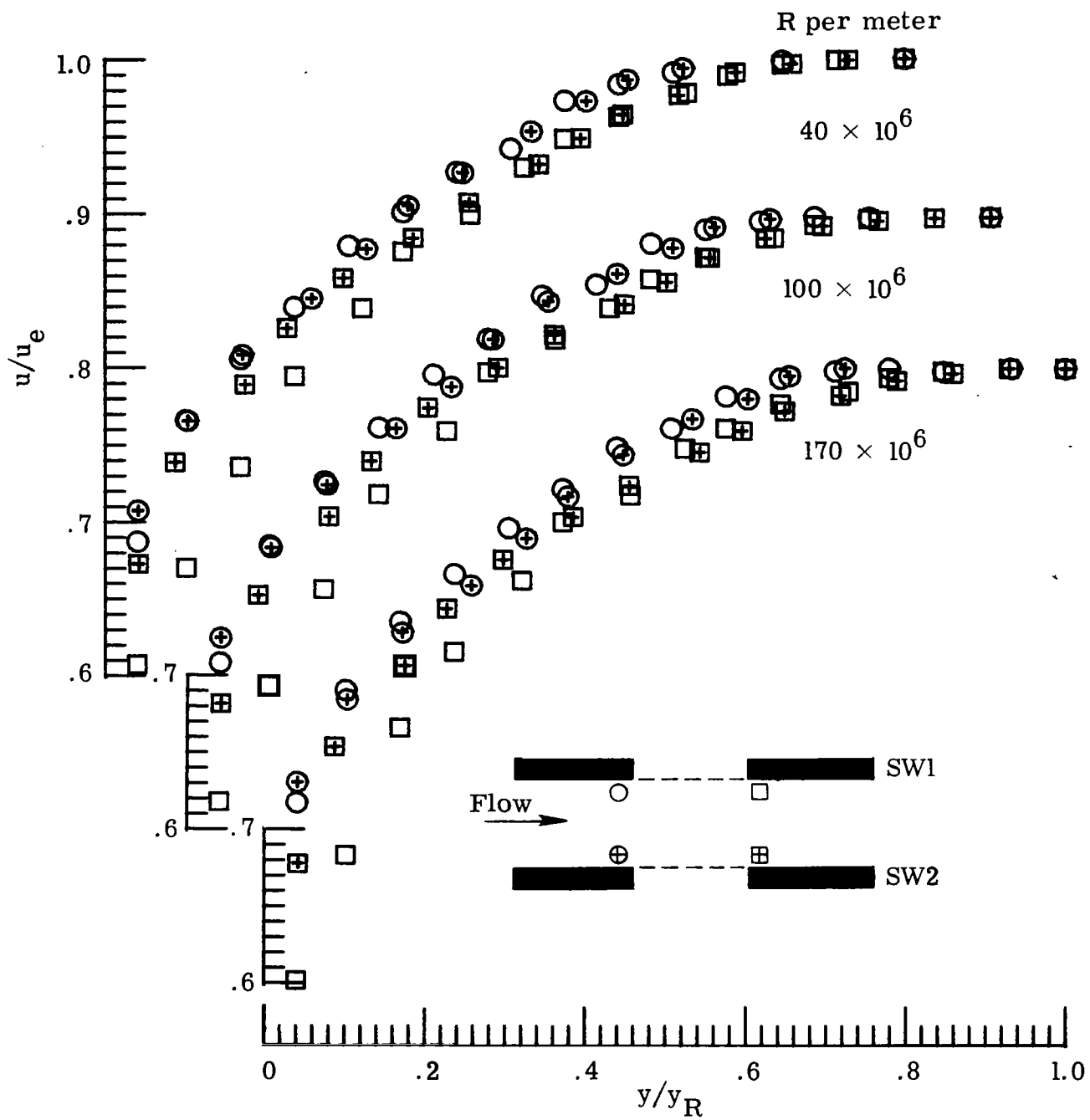
(d) M = 0.70.

Figure 7.- Continued.
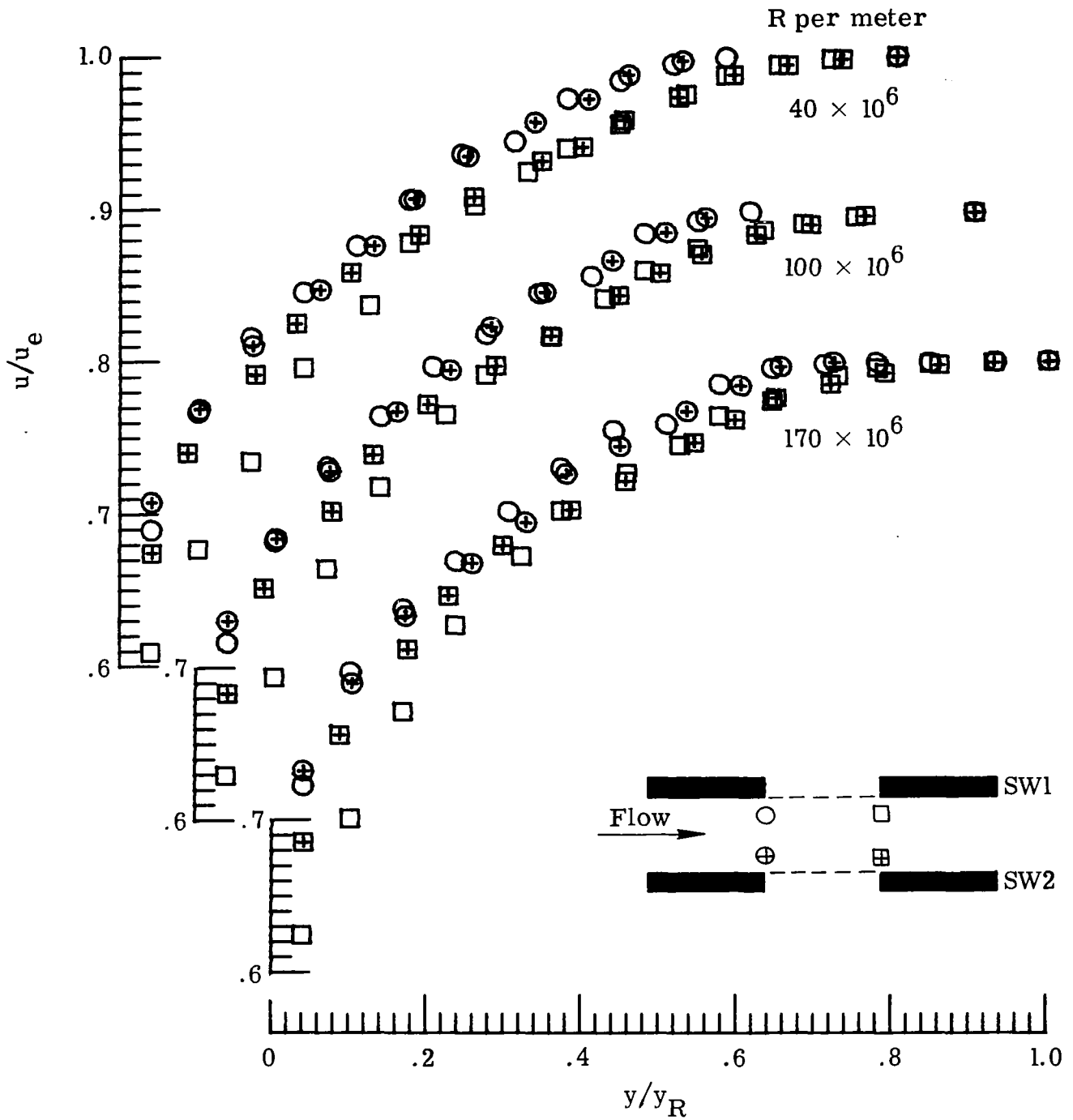
(e) M = 0.76.

Figure 7.- Concluded.
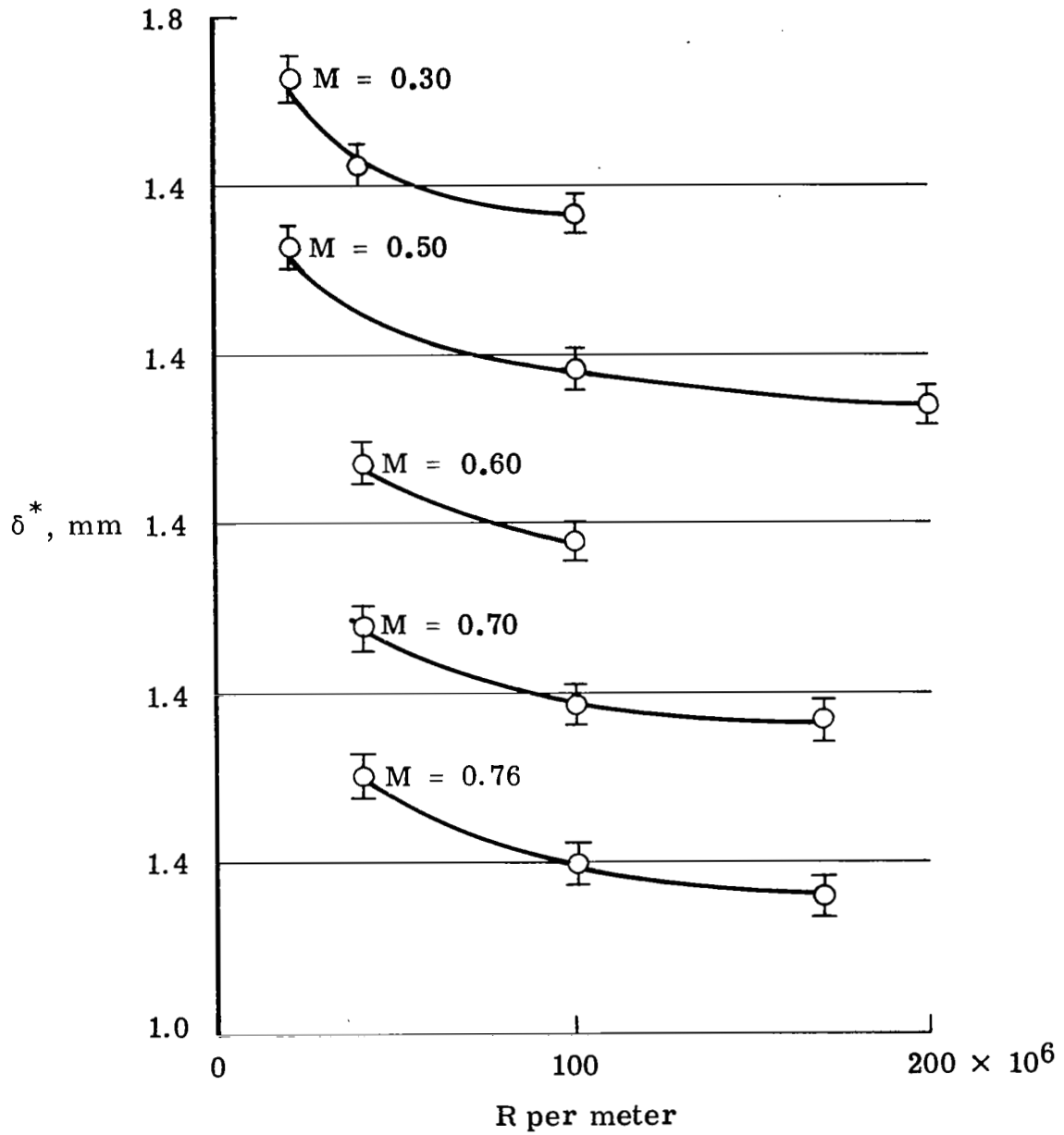
(a) Displacement thickness.

Figure 8.- Effect of Mach number and Reynolds number on sidewall boundary-layer parameters upstream of perforated plate.
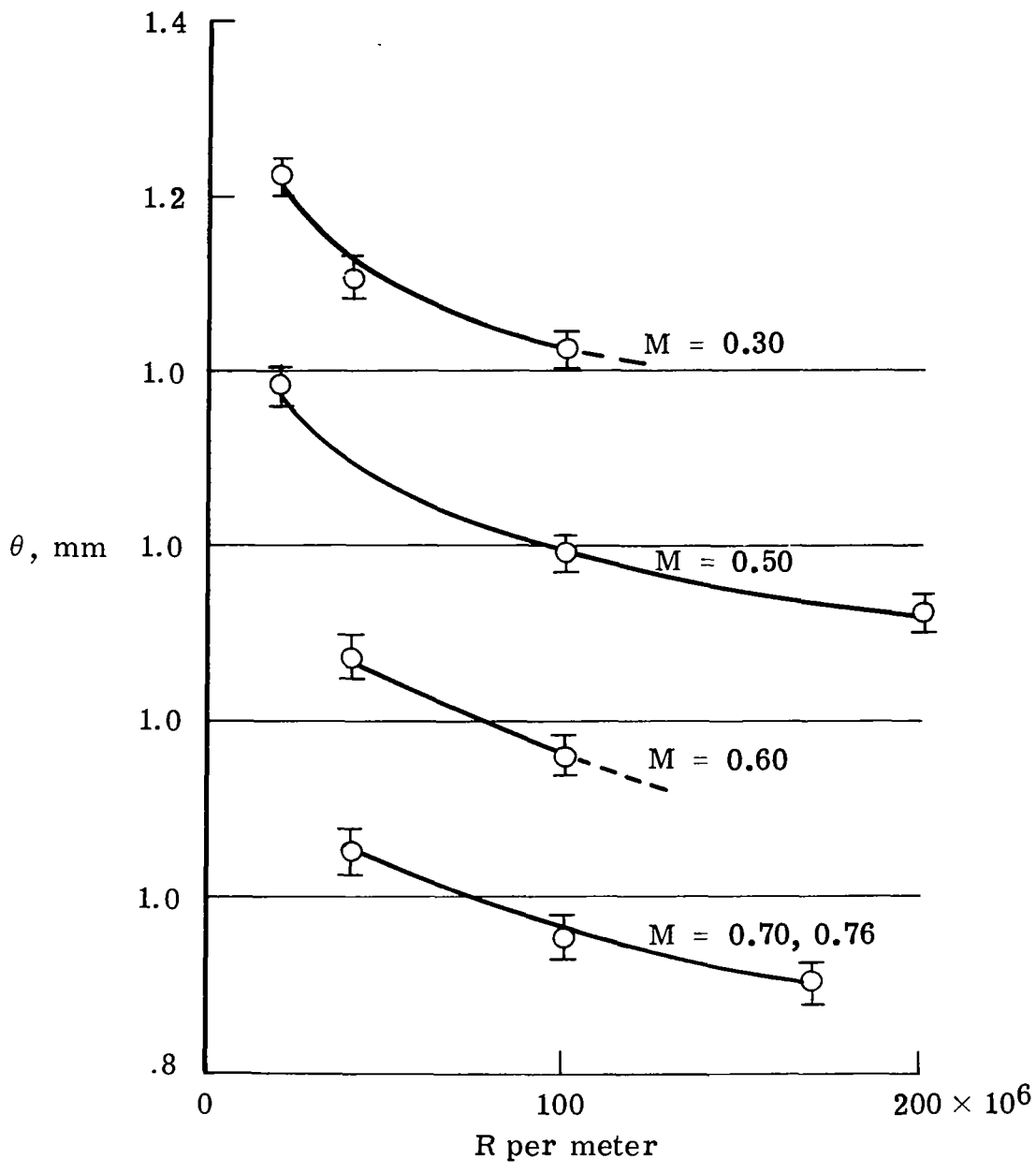
(b) Momentum thickness.

Figure 8.- Continued.
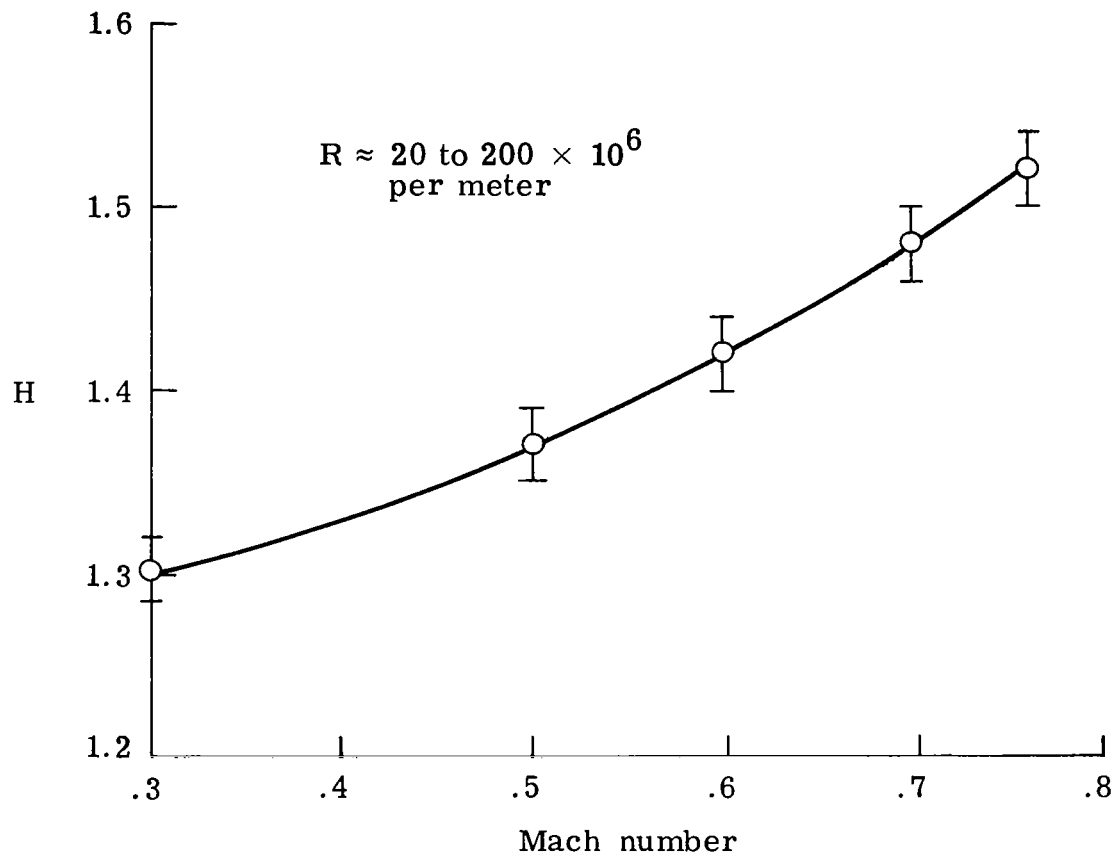
(c) Shape parameter.

Figure 8.- Concluded.
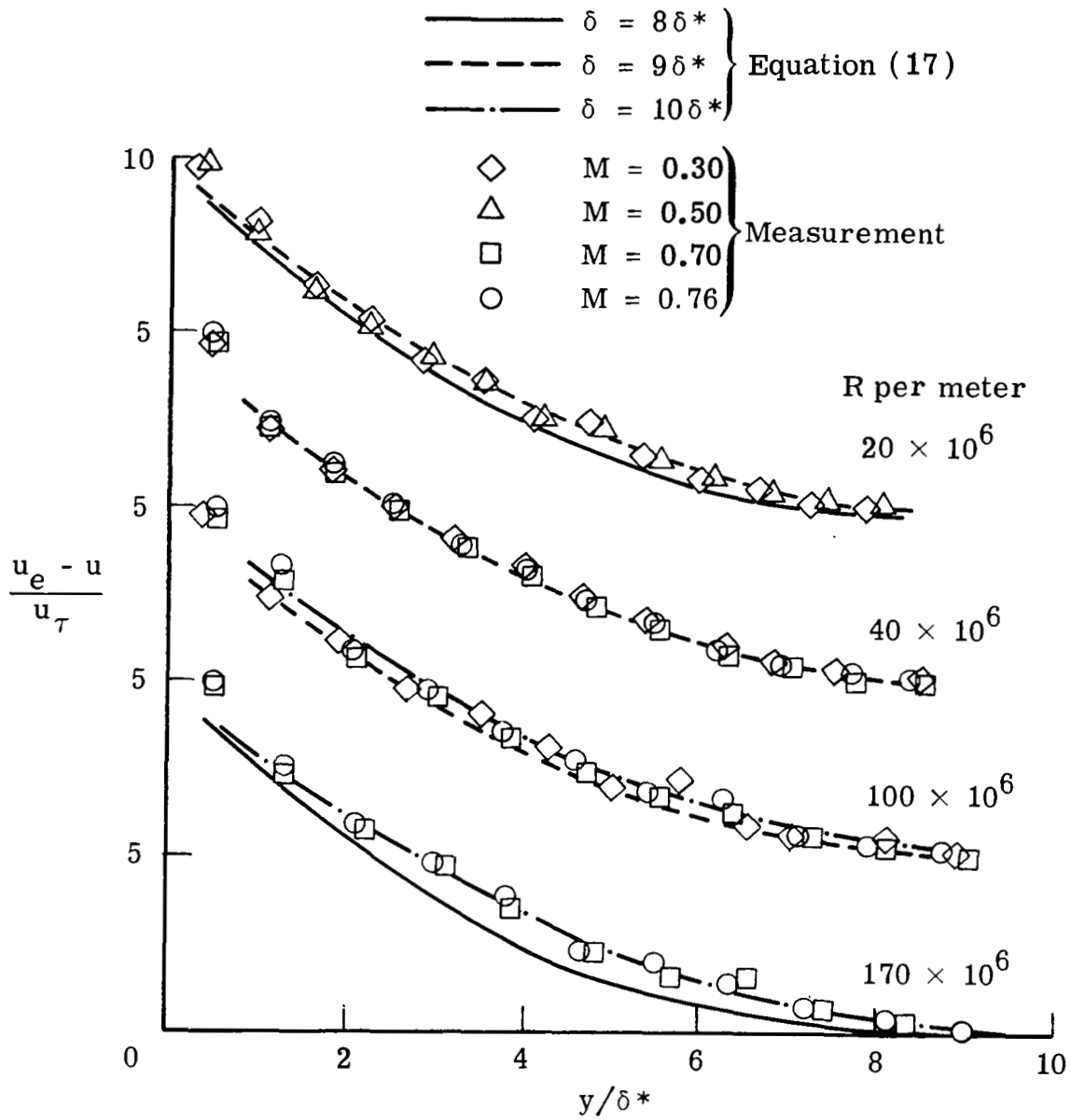
Figure 9.- Correlation of sidewall boundary-layer velocity profiles upstream
of perforated plate with defect law of Hama.
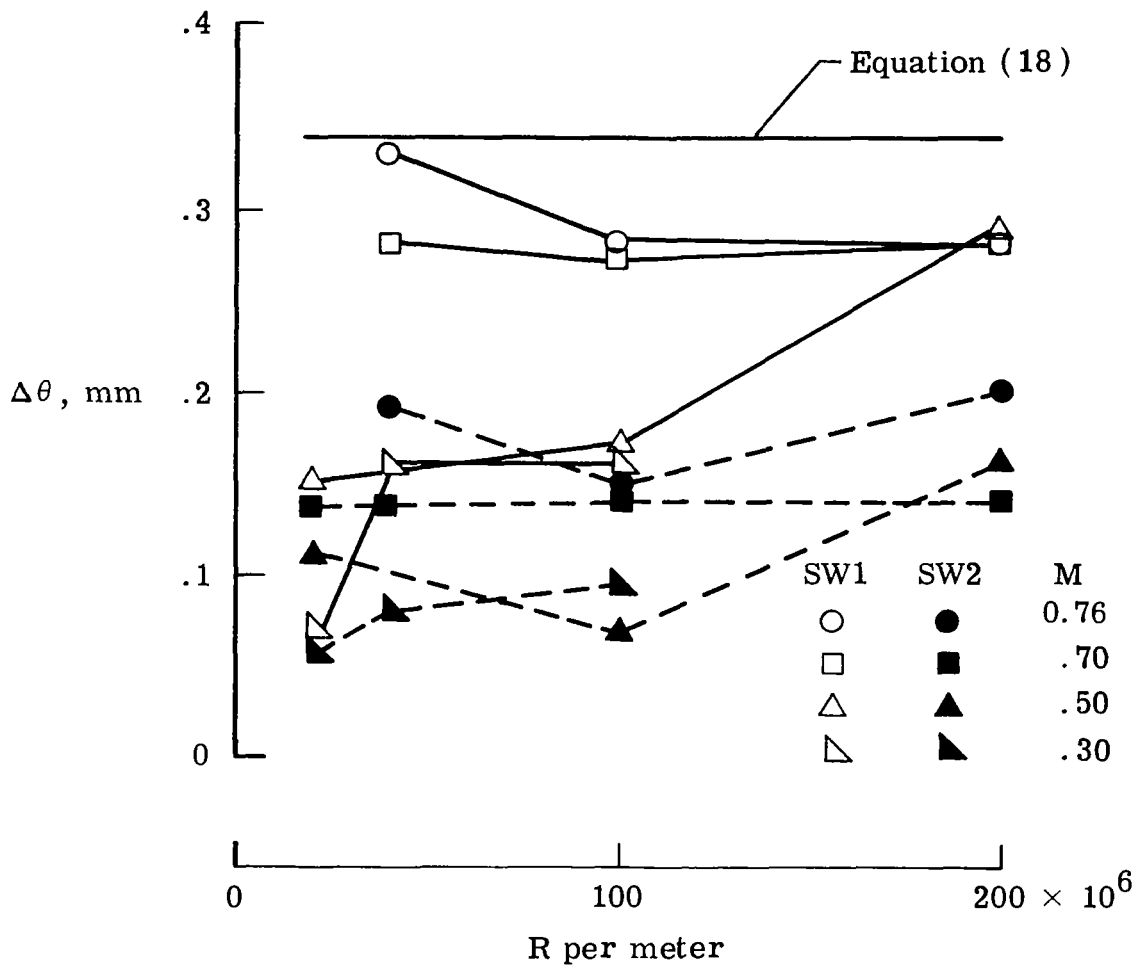
Figure 10.- Increase in momentum thickness across perforated plate with no boundary-layer suction.
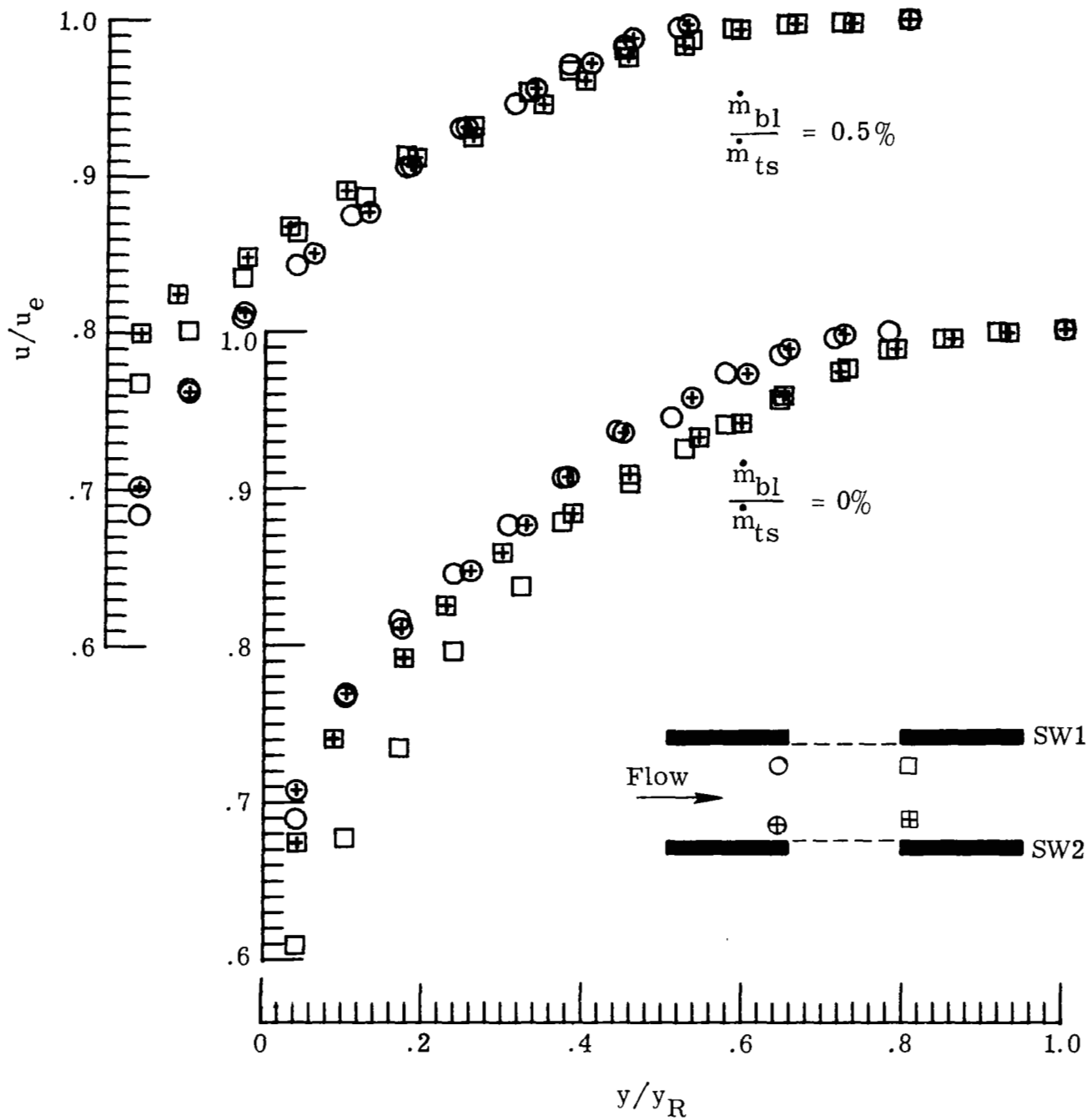
Figure 11.- Effect of boundary-layer bleed on velocity profiles.
Y_R = 15 mm; M = 0.76; R = 40 × 10^6 per meter.
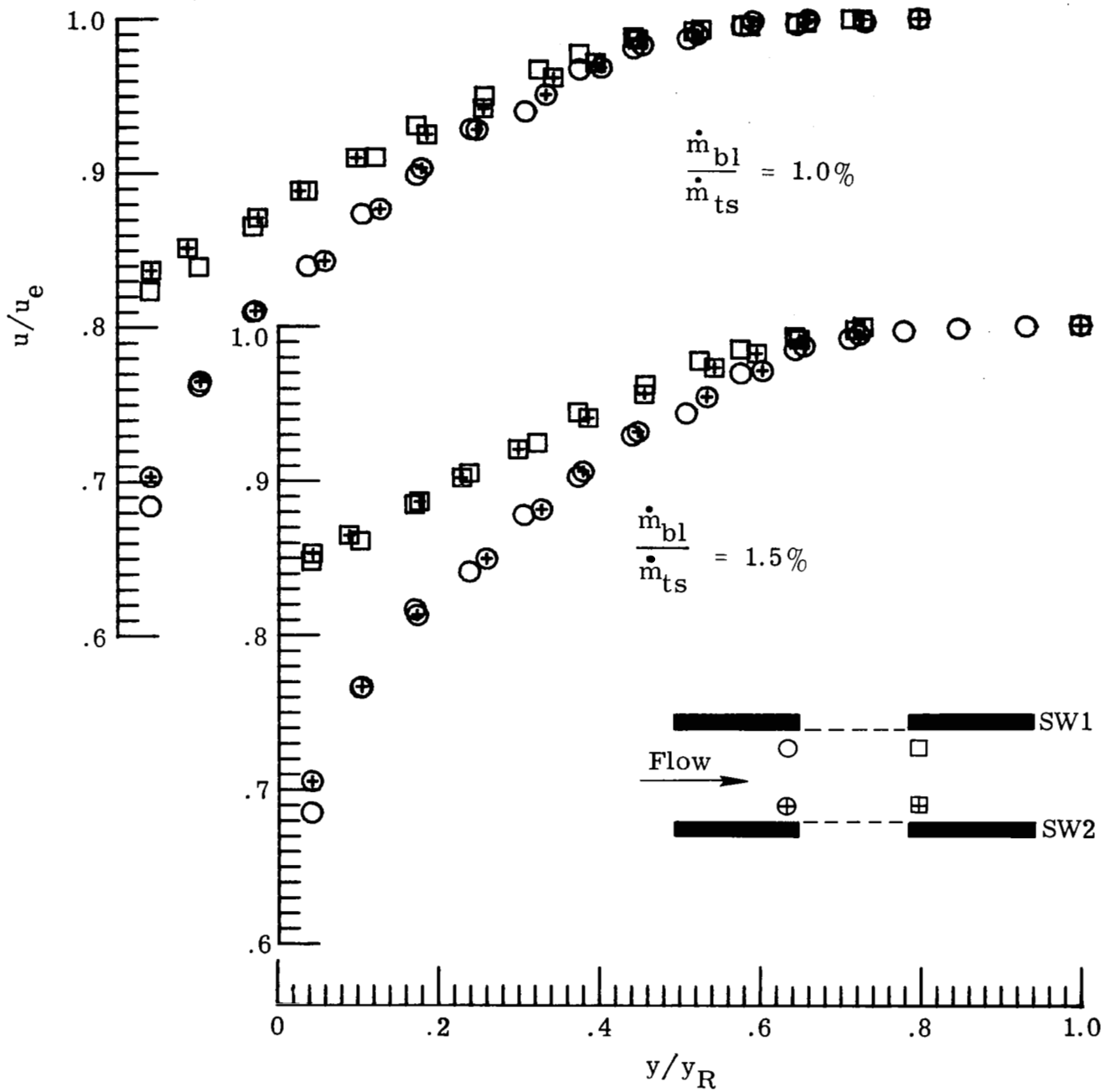
Figure 11.- Continued.
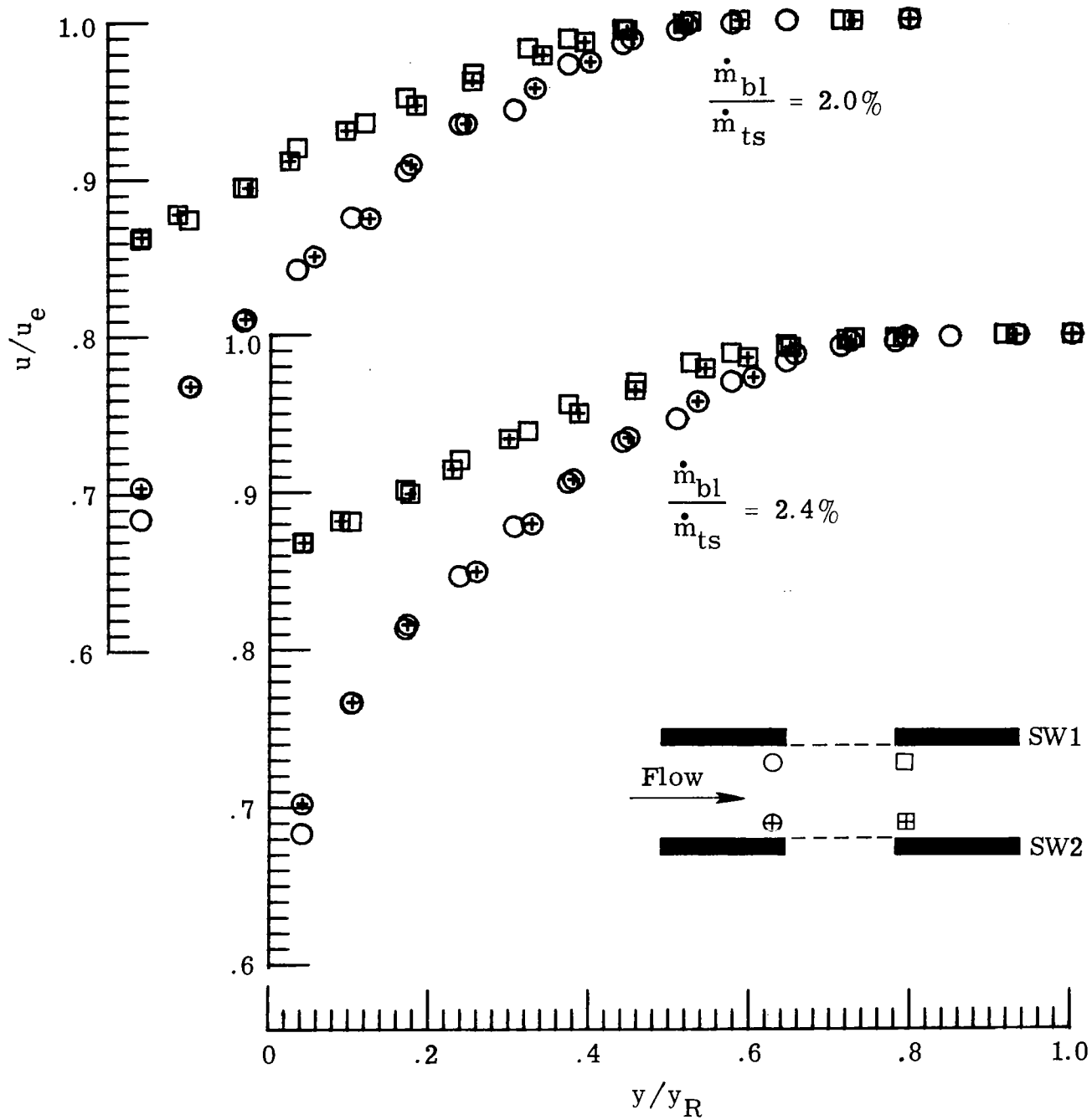
Figure 11.- Concluded.
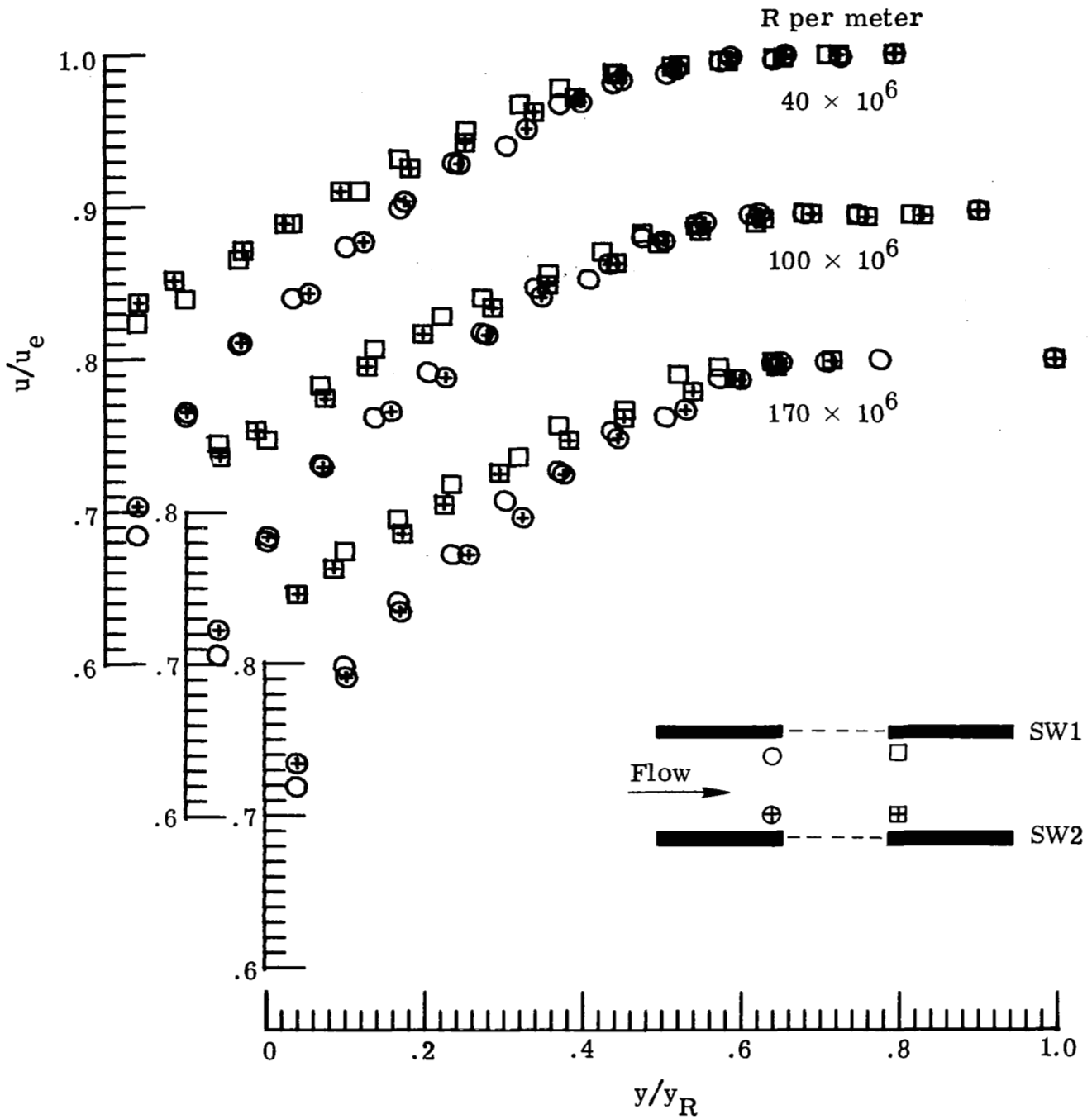
Figure 12.- Velocity profiles for different Reynolds numbers with 1-percent suction. $y_R = 15$ mm; $M = 0.76$.
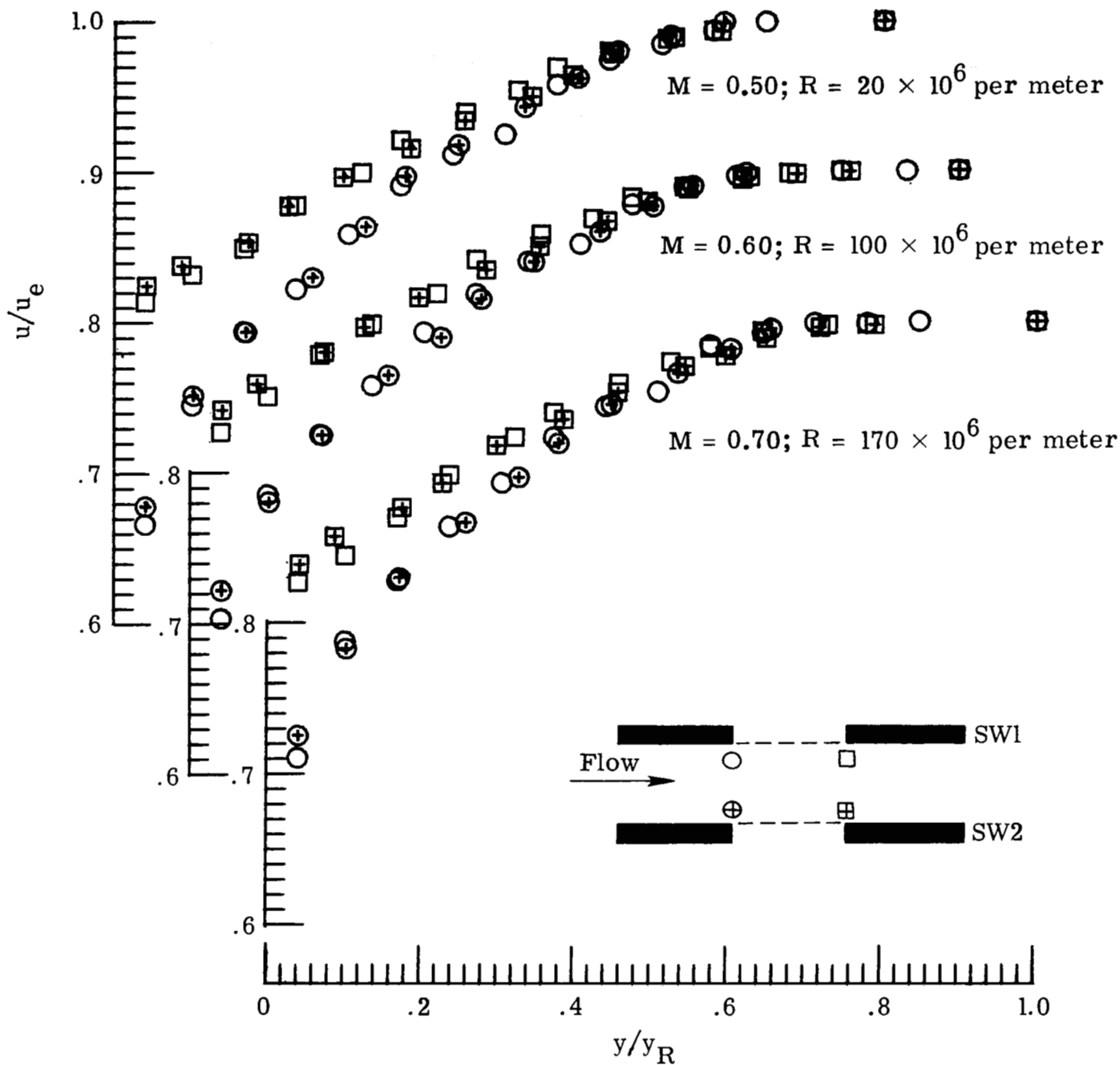
Figure 13.- Velocity profiles for different Mach numbers and Reynolds numbers with 1-percent suction. y_R = 15 mm.
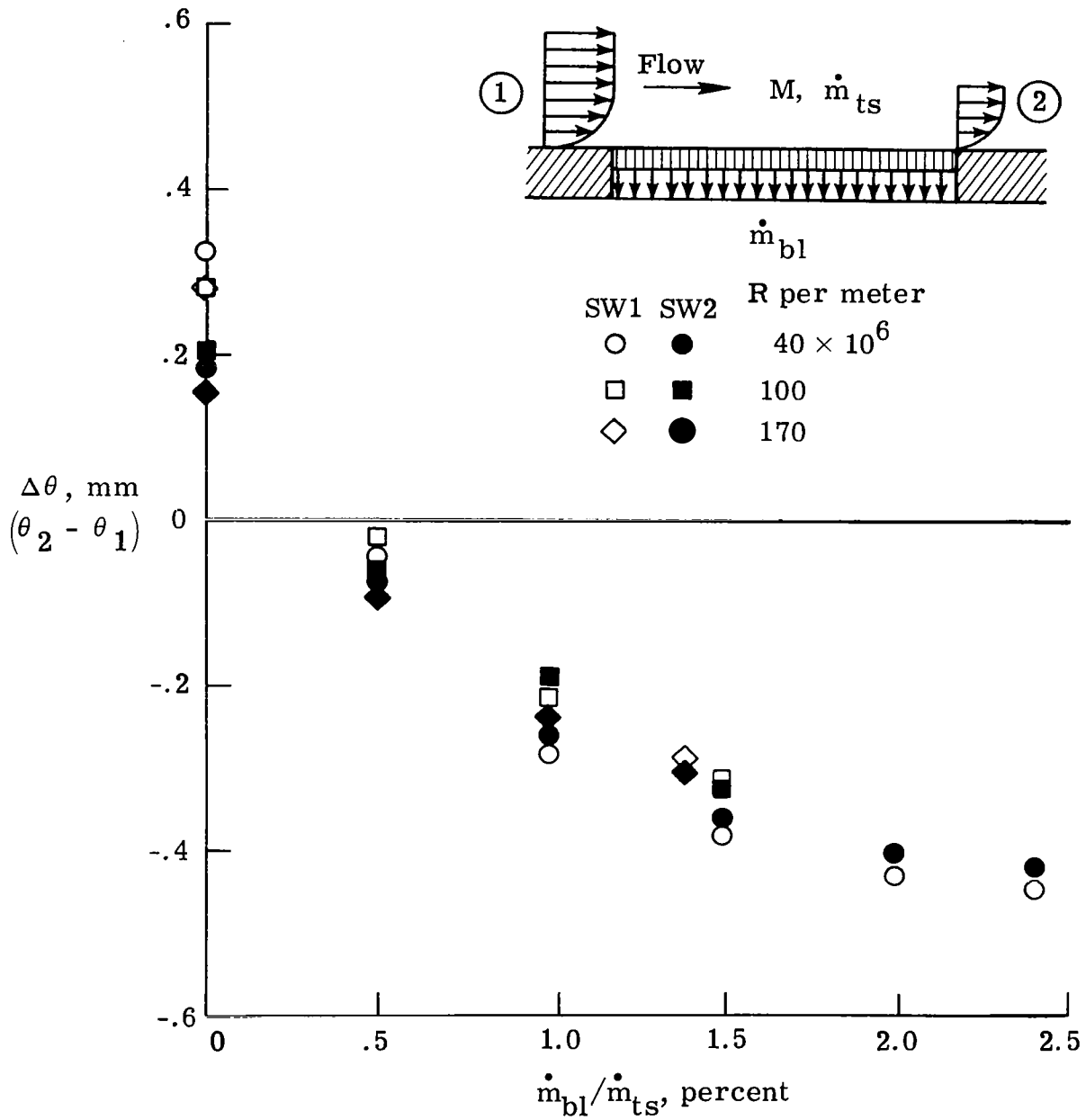
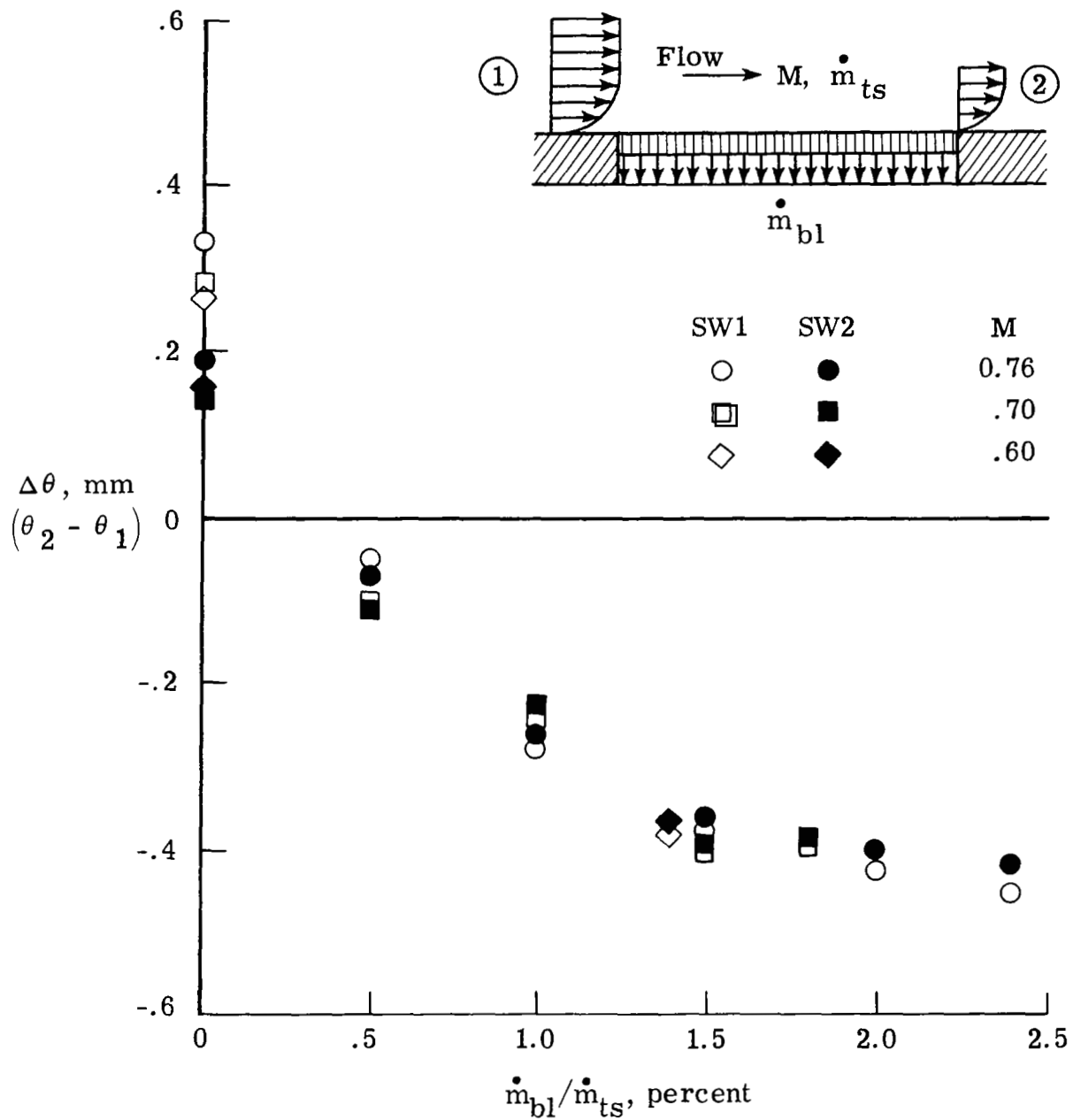Figure 14.- Variation of momentum-thickness increment with suction, including effect of Reynolds number. M = 0.76.

Figure 15.- Variation of momentum-thickness increment with suction, including effect of Mach number. $R = 40 \times 10^6$ per meter.
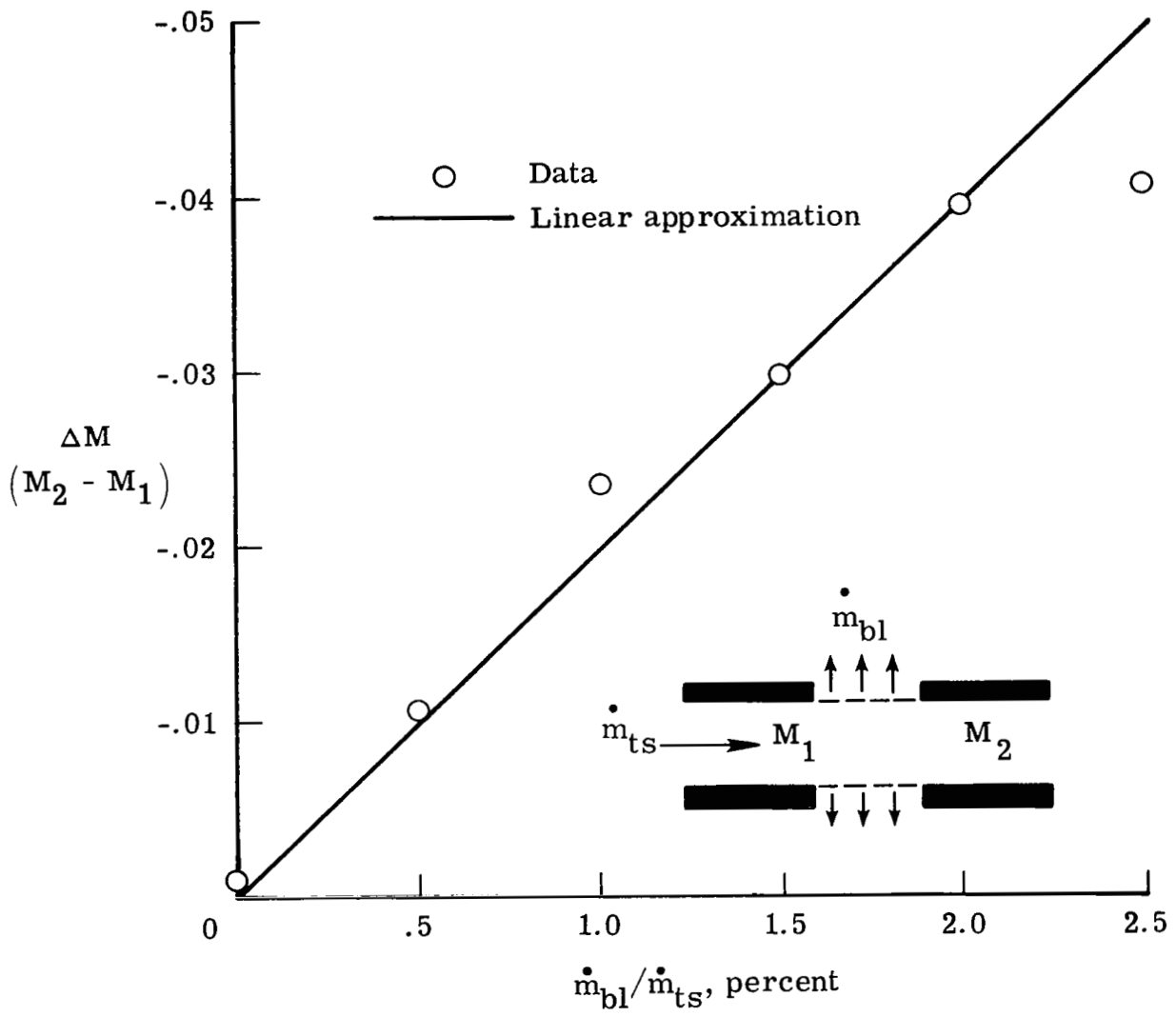
Figure 16.- Change in Mach number across perforated plate due to suction. $M = 0.76$; $R = 40 \times 10^6$ per meter.
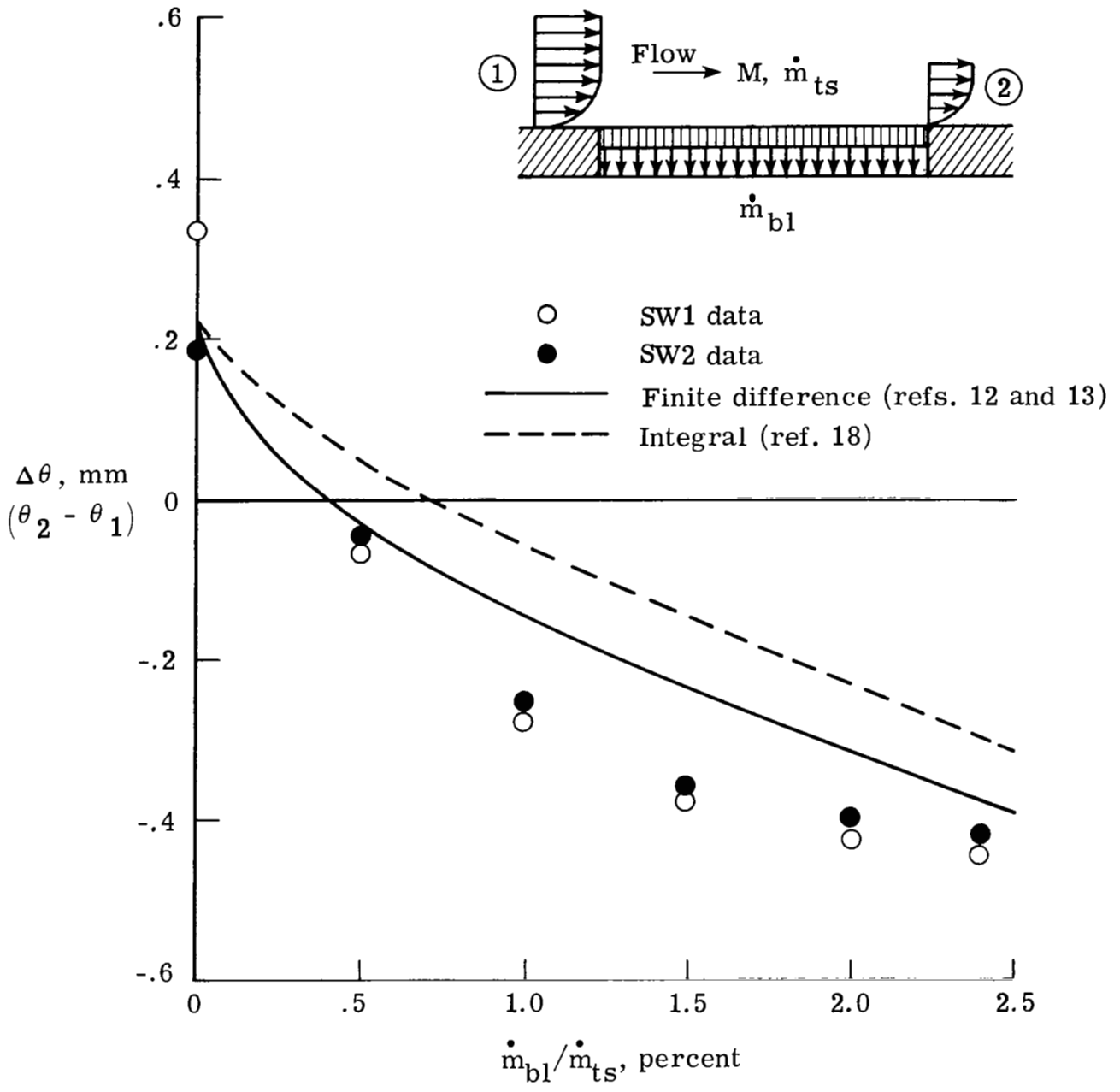
Figure 17.- Comparison of change in momentum thickness with theoretical predictions. $M = 0.76$; $R = 40 \times 10^6$ per meter.
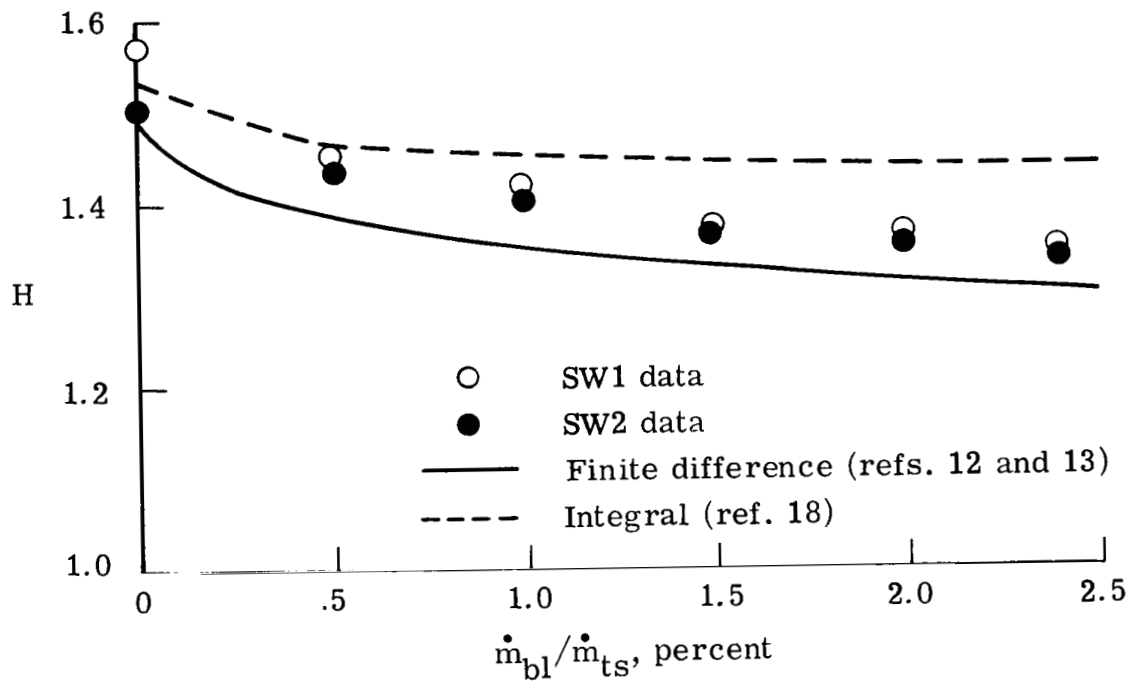
Figure 18.- Comparison of change in shape parameter with theoretical predictions. $M = 0.76$; $R = 40 \times 10^6$ per meter.
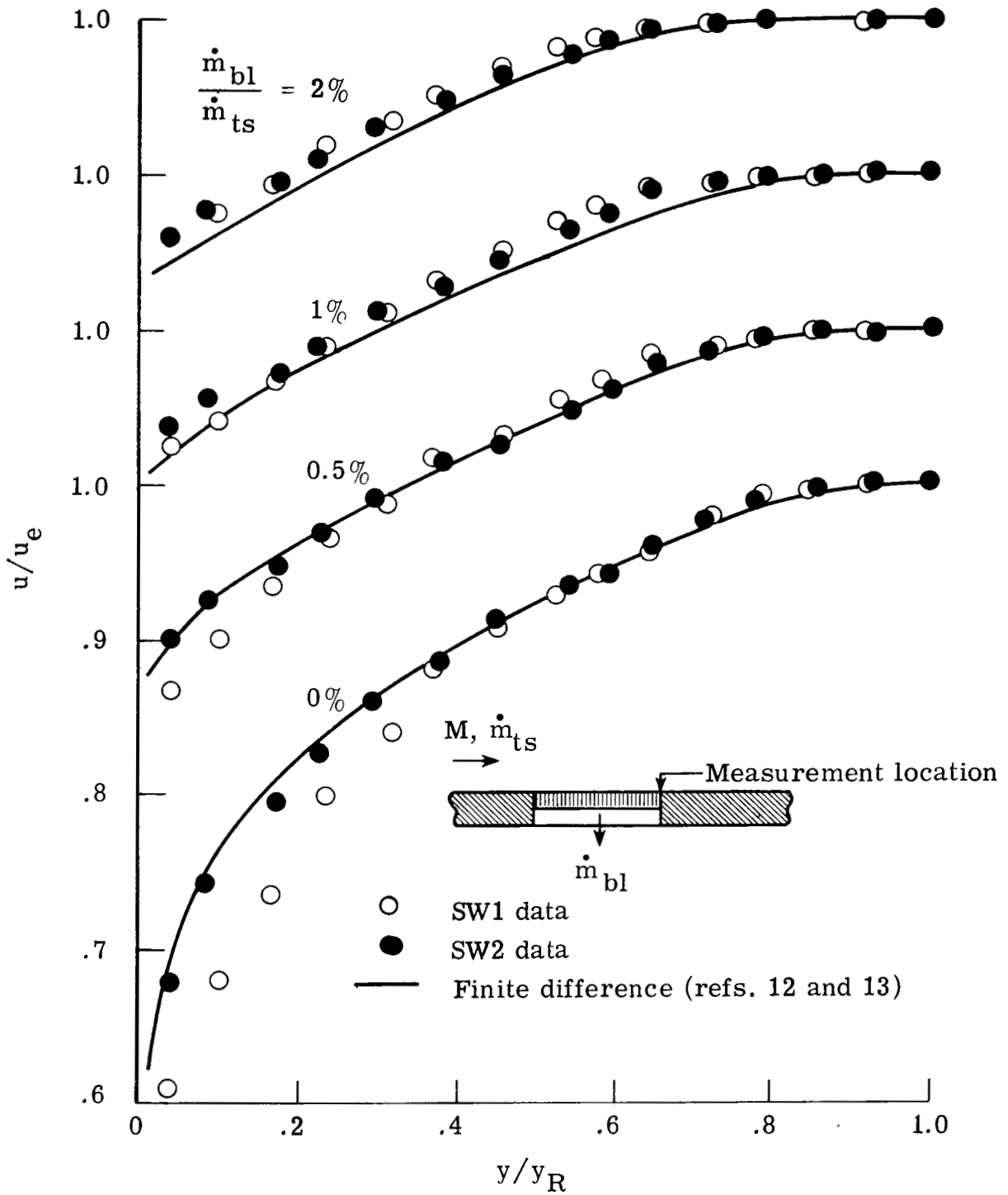
Figure 19.- Comparison of velocity profiles at various suction rates with finite-difference calculations. $M = 0.76$; $R = 40 \times 10^6$ per meter.
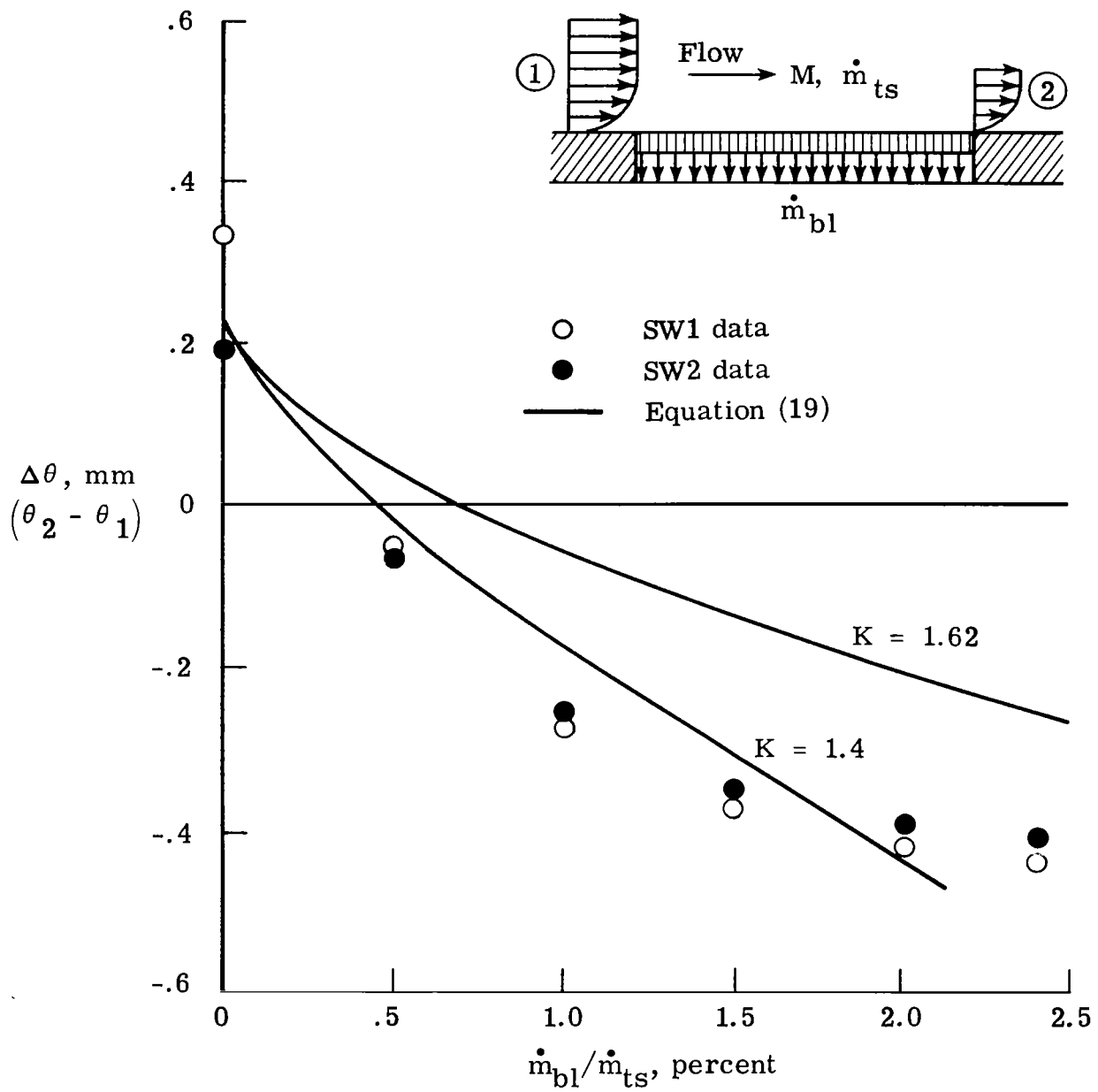
Figure 20.- Comparison of change in momentum thickness with a simplified integral equation. $M = 0.76$; $R = 40 \times 10^6$ per meter.

1. Report No. NASA TP-2096	2. Government Accession No.	3. Recipient's Catalog No.
4. Title and Subtitle STUDIES OF SIDEWALL BOUNDARY LAYER IN THE LANGLEY 0.3-METER TRANSONIC CRYOGENIC TUNNEL WITH AND WITHOUT SUCTION		5. Report Date March 1983
		6. Performing Organization Code 534-02-13-16
7. Author(s) A. V. Murthy, Charles B. Johnson, Edward J. Ray, Pierce L. Lawing, and Jerry J. Thibodeaux		8. Performing Organization Report No. L-15437
		10. Work Unit No.
9. Performing Organization Name and Address NASA Langley Research Center Hampton, VA 23665		11. Contract or Grant No.
		13. Type of Report and Period Covered Technical Paper
12. Sponsoring Agency Name and Address National Aeronautics and Space Administration Washington, DC 20546		14. Sponsoring Agency Code

15. Supplementary Notes

A. V. Murthy: NRC-NASA Resident Research Associate.

16. Abstract

Boundary-layer measurements on the sidewalls of the Langley 0.3-Meter Transonic Cryogenic Tunnel were made to determine the effectiveness of the passive boundary-layer bleed system over a Reynolds number range from 20 to 200×10^6 per meter at Mach numbers from 0.30 to 0.76. It was found that the tunnel sidewall boundary-layer displacement thickness was about 2 percent of the width of the test section without the boundary-layer bleed. Measured velocity profiles correlated well with the defect law of Hama. With the boundary-layer bleed equivalent to about 2 percent of the test-section mass flow, the boundary-layer displacement thickness reduced to about 1 percent of the test-section width, which is generally considered acceptable for testing airfoils. It was also noticed that effectiveness of the bleed was nearly independent of the Mach number and Reynolds number over the range of conditions tested. A comparison of the measured suction effectiveness of the bleed with the finite-difference and integral methods of boundary-layer calculation showed good agreement.

17. Key Words (Suggested by Author(s)) Boundary-layer control Wind tunnels Cryogenic Sidewall boundary-layer removal Nitrogen	18. Distribution Statement Unclassified – Unlimited Subject Category 34
19. Security Classif. (of this report) Unclassified	20. Security Classif. (of this page) Unclassified	21. No. of Pages 48	22. Price A03